University of Venda
Creating Future Leaders

University of Venda

Preparation and characterization of co-doped lithium vanadate solid solutions

by

RAMUKHITHI LIVHUWANI KNITTOR

Student number: 11521016

A dissertation submitted in fulfilment of the requirements for Master of Science in **Chemistry**

School of Mathematical and Natural Sciences

Department of Chemistry

University of Venda

Thohoyandou, Limpopo

South Africa

Student: **Ramukhithi L.K**. Signed  .....

Supervisor: **Dr Legodi M.A.** Signed:  …

Co-supervisor: **Prof Teuns van Ree** Signed: 

Co-supervisor: Dr Sikhwivhilu L.M. Signed: 

© University of Venda

Dedication

Dedicated to my son, Dzivha Maumela.

To my parents, Tshilidzi Yvonne & Azwitamisi Phanuel Ramukhithi, and my siblings, Muneiwa & Thuso, for their endless love, support and encouragement.

© University of Venda

University of Venda
Creating Future Leaders

Declaration

"I declare that the dissertation hereby submitted to the University of Venda, for the degree of Master of Science in Chemistry has not previously been submitted by me for a degree at this or any other university; that it is my work in design and in execution, and that all material contained herein has been duly acknowledged."

Ramukhithi Livhuwani Knittor

Signature:  Date: 24 / 11 / 2020

© University of Venda

Acknowledgements

The research could not have happened without support from many different people who contributed in various ways. Firstly, I would like to give thanks to the almighty God for providing me with good health and inspiration during the research period.

Secondly, thanks to my supervisor Dr Legodi M.A. for his support, guidance and critical comments that he has provided on throughout my research work. Together with my co-supervisors Prof. van Ree T. and Dr Shikhwivhilu L. I would like to thank Mr Maphiri V.M. for his support and doing some characterizations.

The NRF/Sasol scholarship is highly appreciated for financial support. My gratitude is expressed towards the stuff of Mintek (Randburg) for allowing me access to their laboratories and also providing me with advice.

Lastly, I would like to appreciate my family, in particular my mother (Ms T.Y Ramukhithi), together with Vhonani Maumela for their encouragement and support throughout my research work.

© University of Venda

Keywords and acronyms

CS	Carbon sheets
CV	Cyclic voltammetry
EDS	Energy dispersive X-ray spectroscopy
EIS	Electrochemical impedance spectroscopy
FTIR	Fourier transform infrared spectroscopy
FWHM	Full width at half maximum
G	Graphene
GNS	Graphene nanosheets
LIB	Lithium-ion battery
LVO	Lithium vanadate
N-G	Nitrogen-doped graphene
XRD	Powder X-ray diffraction spectroscopy
RS	Raman spectroscopy
SEI	Solid electrolyte interface
SEM	Scanning electron microscopy
XRF	X-ray fluorescence

© University of Venda

Table of Contents

© University of Venda

© University of Venda

List of Tables

© University of Venda

List of Figures

© University of Venda

Abstract

In this study, a class of inorganic materials Li_3VO_4, $Li_{3-x}Na_xVO_4$, $Li_{3-x}K_xVO_4$, $LiV_{1-y}Cr_yO_4$, and $Li_{3-x}K_xV_{1-y}Cr_yVO_4$ (where x = 0.01, 0.05 & 0.1; y = 0.01, 0.05 & 0.1) were effectively synthesized via citrate sol – gel method. Structural properties of the prepared inorganic materials were characterized by powder X – ray diffraction spectroscopy (XRD), Fourier transform infrared (FTIR) spectroscopy, Raman spectroscopy (RS), Scanning Electron Microscopy (SEM) and Energy dispersive X – ray spectroscopy (EDS).

The XRD data showed that the synthesized materials have an orthorhombic crystal structure (space group Pmn21). From the obtained XRD data, different structural parameters (a, b, and c) are also suggested. The Fourier transform infrared (FTIR) spectroscopy analysis showed one distinct strong absorption peak at 600 – 950 cm^{-1} due to the bending vibrations of the V – O – V bonds of VO_4 tetrahedron. Raman study of un – doped and doped lithium vanadate, shows two distinct strong Raman modes which represent VO_4 tetrahedra are identified in the Raman shift region of 790 cm^{-1} to 830 cm^{-1}. The Energy dispersive X – ray spectroscopy (EDS) analysis shows the presence of vanadium and oxygen for undoped LVO, vanadium, oxygen, and sodium for Na-doped LVO, vanadium, oxygen, and potassium for K-doped LVO, vanadium, oxygen, and chromium for Cr-doped LVO and for K & Cr-doped LVO, vanadium, oxygen, potassium, and chromium are present. Surface morphology of the pure and doped Li_3VO_4 was examined by SEM and the average particle sizes were in between 600 nm and 1000 nm.

© University of Venda

Chapter 1: Introduction

1.1 Background

The shortage of fossil fuels and environmental pollution affects social activities, as exploitation of sustainable energies such as tidal energy, solar and wind gets the ever-increasing attention. Therefore, the uncontrollability and discontinuity of these energies need complicated energy storage systems (Armand *et al.*, 2008; Goodenough *et al.*, 2009)). Among the different types of energy sources available to us, batteries find a superior position because they play a vital role in the sector of portable electronics (like laptops, cell-phones), medical applications and even electric vehicles (hybrid and non-hybrid), plug-in electric vehicles (Mo *et al.*, 2017). Due to their high operating voltage, friendly environment compatibility, high capacity, and lithium – ion batteries (LIBs) are regarded as the most promising energy storage devices (Zhu *et al.*, 2013). Currently, LIBs with superior safety, better cycling performance, and higher energy density are required.

A battery is a closed system for electrochemical energy conversion and storage. It consists of : anode, cathode and electrolyte. Batteries are devices for storing power from energy sources, for example, fossil fuels or renewable resources, for future use. Secondary batteries are known as rechargeable batteries, are becoming more popular because of their ability to charge and discharge multiple times, thereby eliminating the need to buy new batteries every time a device is flat or fully discharged (Bellis, 2012).

The development of mobile electronic devices (.i.e. cell-phones, laptops, and video cameras) throughout the 1980s led to a growing demand for secondary batteries with greater capacity than secondary batteries that were under development at the time, namely: lead – acid, nickel – cadmium (NiCd) and nickel – metal hydride (NiMH) batteries, posed limitations to the reduction in weight and size (Yoshino, 2012). Therefore the need remains for a new, small, and lightweight secondary rechargeable battery (Yoshino, 2012).

© University of Venda

As shown in **Table 1.1**, there are two main classifications for batteries, that is, primary (disposable) and secondary (rechargeable). Furthermore, batteries can be classified as either aqueous or non-aqueous, depending on the type of electrolyte they use.

Table 1.1: Types of batteries (Yoshino, 2012)

	Aqueous electrolyte battery	**Non-aqueous electrolyte battery**
Primary battery	Alkaline dry cell	Metallic lithium battery
Secondary battery	Lead – acid battery Nickel – cadmium battery Nickel – metal hydride battery	**Lithium-ion battery**

Lithium – ion batteries (LIBs) were introduced to the market by Sony Corporation in 1991 (Kalluri, 2016) and consisted of two electrodes, a negative anode, and positive cathode and an electrolyte utilized for the transfer of lithium ions between electrodes (Davison, *et al*., 2012). LIBs have shown significant progress concerning safety and electrochemical properties like power, cycling stability, and capacity. When compared to other secondary batteries like nickel-metal hydride and nickel-cadmium, LIBs have the highest energy density (Bensalah, 2016).

Lithium-ion battery consists of an anode (negative electrode), cathode (positive electrode), electrolyte, and separator. During the discharge, the anode is oxidized and releases electrons while the cathode receives electrons and is reduced during the discharge. The anode and cathode are physically separated by a separator material. The electrolyte is an ionic conductor but an electronic insulator which provides good ionic conductivity to transfer the lithium ions (Li^+ ions) during charge/discharge processes to prevent short-circuiting. The electrolyte is a lithium salt in an organic solvent and Li_3VO_4 (LVO) can also be utilized as an electrolyte (Kim *et al.*, 2013). The separator is a porous polymer which is an electrically insulating material

© University of Venda

which prevents the direct contact of the two electrodes (anode and cathode), while allowing ionic conduction.

During the discharge process, lithium atoms lose their outer conduction electron to form energetically favoured lithium ions with a complete inner shell of electrons. The lithium-ion formed moves towards the cathode material developing a concentration gradient of the ions in this half of the cell. However, this process results in an increasingly large negative charge at the anode. Thus, the flow of lithium ions would soon stop because the charge of the remaining conduction band electrons are not self-discharging. The supply of cast-off electrons is put to work by connecting a load (electricity consuming device) externally between the anode and cathode as shown in Figure 1.1. By doing so, the electrons also get to the cathode through an external circuit where they neutralize some of the lithium ions. Thus, more lithium atoms in the anode are now free to leave behind their conduction electrons and join the flow towards the cathode. During charging (by applying an external voltage), the process gets reversed. Now the cathode material gives up lithium ions that de-intercalates from the cathode and intercalate or diffuse back into the anode, thus “recharging” makes the lithium-ion battery ready to power a load again.

© University of Venda

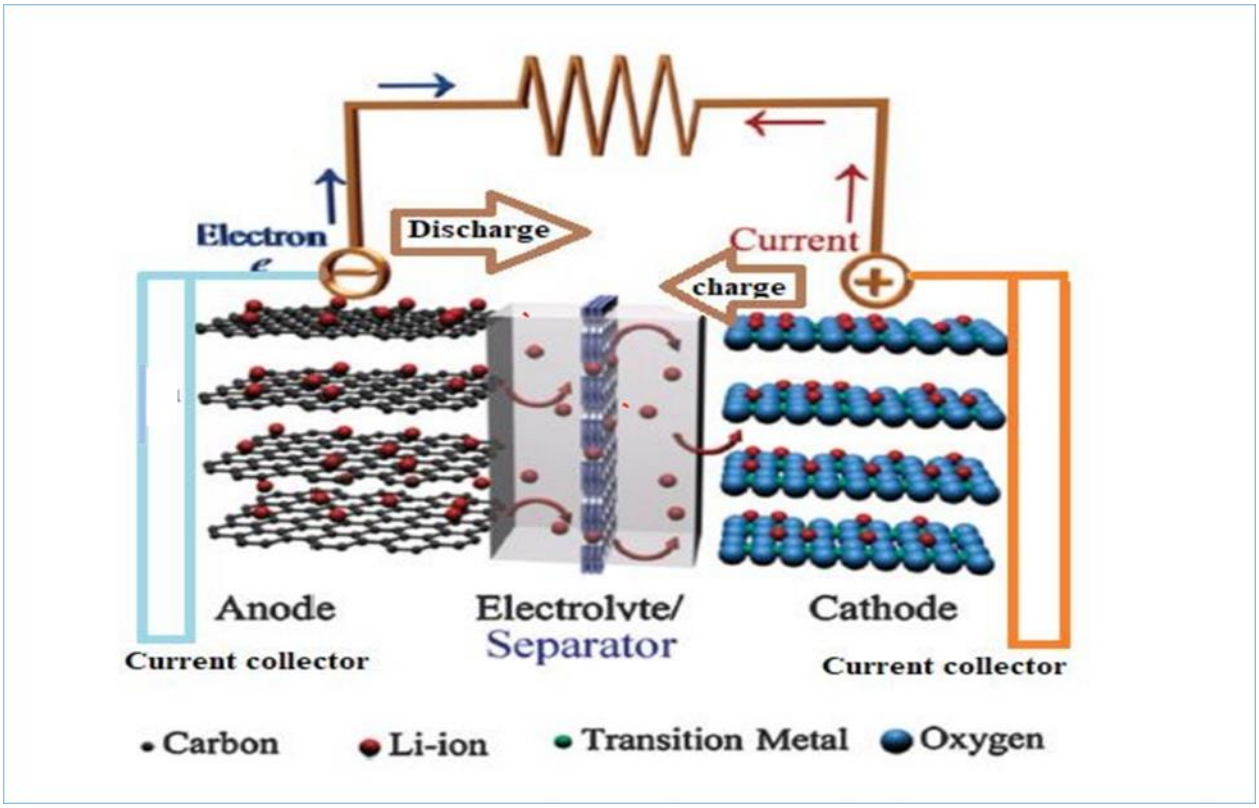

Figure 1.1: Representation of LIB operation during charge and discharge process (Bhatt *et al*., 2015)

Due to the current wide use of lithium – ion batteries, it was found that the advantages of these batteries far outweigh their disadvantages. LIBs are environmentally friendly (contain less toxic metals), are self-discharging, and have low maintenance (no periodic discharge is needed). They have good charging performance at low temperatures (Bhatt *et al.*, 2015). Lithium-ion batteries have specialty cells that provide very high current to applications like power tools. Also, different types of LIBs are available (Bonheur, 2016). However, lithium-ion batteries require a modulator (or circuit) to regulate voltage and current within safe limits. They are not cheap to manufacture and also age with time (Bonheur, 2016).

Numerous synthesis techniques (Figure 1.2) have been developed and use to fabricate cathode electrode materials for LIBs includes sol – gel method (Zhang, 2015), solid-state reaction (Liu *et al.*, 2009), hydrothermal synthesis (Luo, 2016; Zou, 2016), soft-combustion process (Prabaharan *et al.*, 2001), chemical polymerization (Zhang, 2015) and many others.

© University of Venda

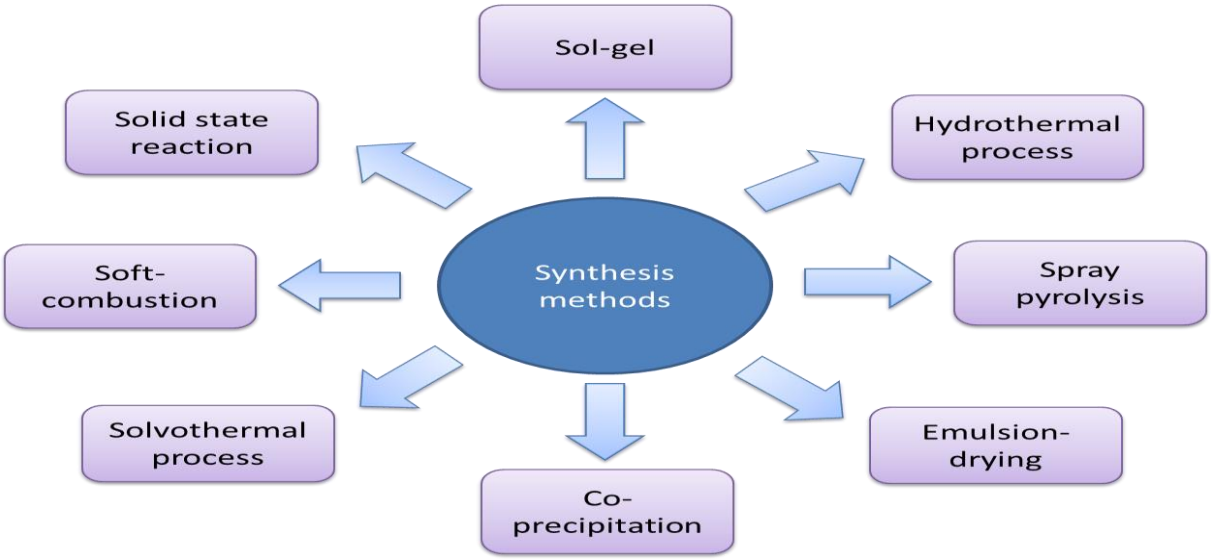

Figure 1.2: Different methods for synthesizing anode materials

The morphological properties like surface texture, grain size, crystallinity, size distribution as well as electrochemical properties of materials formed, like capacity retention rate, initial discharge, and cyclability, are directly affected by the synthesis method.

Characterization of the prepared anode materials was undertaken using various techniques. These techniques included powder X – ray diffraction (XRD), Fourier Transform infrared (FTIR) spectroscopy, scanning electron microscopy (SEM), X – ray fluorescence (XRF), energy – dispersive X – ray spectroscopy (EDS) and thermal gravimetric analysis (TGA). These analysis techniques were used to examine crystal structures, functional groups, chemical and phase composition, surface morphology, thermal stability of synthesized materials (Ni *et al.*, 2014).

Recent work has shown that due to the vanadium states across the Fermi energy, vanadate – based electrode materials have metallic response. Therefore, they have the advantage of high electronic conductivity (Chakrabarti *et al.*, 2017). Among other vanadates, Li_3VO_4 requires further modifications because it's low electronic conductivity which leads to polarization and very poor rate capability. In this work, we propose co-doping of lithium vanadate on the lithium and vanadium ion sites using dopants such as sodium, potassium, and chromium to help

© University of Venda

improving the electronic conductivity and the poor rate capability of the lithium vanadate (Li_3VO_4) electrode material.

1.2 Problem Statement

Dispersed – type energy storage systems, increasing demandifor high energy density and safe rechargeable battery for mobile electronic devices (like cell phones, laptops, cameras, etc.) and electric vehicles have promoted the development of lithium-ion batteries. Recently, new vanadium – based oxide, Li_3VO_4 (LVO), has attracted overwhelming attention in LIB application. Lithium vanadium oxide has much higher capacity, high Li^+ ionic mobility, insignificant structural and volumetric changes during the charge and discharge (lithiation and delithiation) processes (Whittingham, 2004; Wu, 2015 and Zhou *et al.*, 2018). However, lithium vanadate suffers from poor electronic conductivity leading to large polarization, hence poor rate capability. Different methods can be used to improve electronic conductivity, and thus many attempts were made to enhance the electronic conductivity of Li_3VO_4. In this study, LVO was doped with sodium or potassium on the lithium-ion sites and also with nickel or chromium on the vanadium ion sites in an attempt to improve electronic conductivity and rate capability. In doing so, the electronic conductivity of the LVO electrode material is expected to improve.

In the present study, Li_3VO_4, $Li_{3-x}Na_xVO_4$, $Li_{3-x}K_xVO_4$, $Li_3V_{1-y}Cr_yO_4$, and $Li_{3-x}K_xV_{1-y}Cr_yO_4$ materialsiwere synthesized via citrate sol – gel method. Structural and electrochemical performances of these prepared materials were investigated. To the best of our knowledge, $Li_{3-x}K_xVO_4$ and $Li_{3-x}K_xV_{1-y}Cr_yO_4$ materials have not been previously reported.

1.3 Study Rationale

Globally, there is a large concern about climate change as a result of using of fossil fuels. The use of fossil fuels produces large quantities of greenhouse gasses (.i.e. carbon dioxide (CO_2), carbon monoxide and other) to the environment. Therefore, the use of renewable alternative energy sources, (namely: solar, nuclear, wind power, and others), would lower our need to depend on fossil fuels, thus reducing CO_2 emissions. Furthermore, devices to store this energy are needed. The rechargeable LIB is a promising candidate for such devices. The main goal is

© University of Venda

to synthesize materials with improved electrochemical properties, longer cycle life, higher lithium storage capacity, and improved conductivity, and rate capabilities, among others.

1.4 Aim and Objectives

1.4.1 Aim of the study

To synthesize co-doped $Li_{3-x}A_xV_{1-y}B_yVO_4$ (where A = Na or K and B = Cr) solid solutions with improved electrochemical properties, mainly conductivity, using the citrate sol-gel method.

1.4.2 Objectives of the study

- To synthesize undoped Li_3VO_4, singly-doped $Li_{3-x}Na_xVO_4$, $Li_{3-x}K_xVO_4$, $LiV_{1-y}Cr_yO_4$, and co-doped $Li_{3-x}K_xV_{1-y}Cr_yVO_4$.
- To analyse composition, size, crystallinity, thermal stability, and functional groups of undoped Li_3VO_4, singly-doped $Li_{3-x}Na_xVO_4$, $Li_{3-x}K_xVO_4$, $LiV_{1-y}Cr_yO_4$, and co-doped $Li_{3-x}K_xV_{1-y}Cr_yVO_4$ using EDS, SEM, XRD, and FTIR.

1.5 Dissertation layout

The study was conducted in an air atmosphere with samples synthesized in powder form by citrate sol-gel method and it focused on single and co-doping on alkali metals and/or transition metals. Five materials have been selected for the study. Characterization techniques were restricted to available instruments. However, there is a scope for further studies in the future on these types of materials. Generally, this dissertation is subdivided into five chapters. In Chapter 1 the research background, problem statement, study rationale, aim and objectives, and dissertation layout are discussed. In Chapter 2 the literature review is discussed. In Chapter 3, the experimental techniques including a list of chemicals, synthesis techniques, characterization techniques of the samples are outlined. Chapter 4 presents the experimental results from XRD, Raman, FTIR, EDS, and SEM. Finally, Chapter 5 consists of a conclusion and future work.

© University of Venda

Chapter 2: Literature Review

This chapter deals with literature review of the present study. It provides a general background on lithium, vanadium, sodium, potassium, chromium and their properties and uses. It highlights on the general background of lithium vanadate, its disadvantages as an anode electrode material. In summary, this chapter also focuses on vanadium-based electrode materials and how to enhance the electrochemical behaviour of Li_3VO_4. Different synthesis methods are also briefly discussed.

2.1 Background

Lithium is a curial component in the fabrication green energy storage technologies and is also rapidly becoming an important metal. On the periodic table, lithium is the third metal under the alkali group with an atomic mass of 6.94 g/mol and a atomic radius of 1.33 Å and has a boiling point and melting point of 1342 °C and 180.5 °C, respectively. Compared with other alkali metals, Li is the most polarising and electronegative than hydrogen. Therefore, it can accumulate chemical energy very better. Li has a single valence electron which is freely given up for reaction to occur. It has an electron configuration of [He] $2s^1$. Li is mostly used in the rechargeable batteries application for mobile phones, digital cameras, laptops, etc. it is also used for non-rechargeable batteries for things like television remotes, clocks, toys, etc. (Emsley, 2011).

Vanadium (V) is a transition metal from the d – block, appearing between titanium and chromium. Its electron configuration is [Ar] $3d^3$ $4s^2$ (Emsley, 2011). Vanadium is silver in colour with two stable isotopes (^{50}V and ^{51}V) having atomic abundance of 0.25 and 99.75 %, respectively. V has oxidation states range from 2+ to 5+ and in the lithosphere, V occurs in the V^{3+} form, whereas V^{4+} prevails under V^{5+} in the oxidizing conditions. V^{3+} is more stable than V^{2+} (which is unstable in ambient environment, because it can be oxidize by oxygen). Based upon geometry and environment, the ionic radius is between 36 and 79 pm. The V has a high melting_point of 1910 ℃ and its redox chemistry in renewable energy technologies is using different oxidation_states to store electrochemical potential_energy (Moskalyk and Alfantazi, 2003). V is one of the mostly used alloy element for strengthening steels used in the construction of building and bridge.

© University of Venda

Sodium (Na) is a soft metal that easily oxides when exposed to air and reacts vigorously with water. Na is an element located on group 1 and period 3 on the periodic table and has an electron configuration of [Ne] $3s^1$. Na has a boiling point of 882.94 ℃. Na salts are useful more than the Na metal itself and the most common Na compound is sodium chloride (NaCl, common known as table salt) and sodium carbonate (Na_2CO_3) used as a water softener (Emsley, 2011). Na is one of the most abundant element on the planet, makes up to almost 3 % of the Earth's crust.

Potassium (K) is an element of group 1 within the periodic table. This alkali metal is indispensable from both plant and animal life and it has an atomic number and weight of 19,3 and 9.098 g/mol, the boiling point is around 760 ℃ and electron configuration of [Ar] $4s^{1.}$ Potassium has oxidation states +1 and -1, although -1 rarely occurs. K is soft and white metal with silvery lustra and melting point of 63.28 ℃. K is also abundant like Na with 2.4 % of the Earth's crust mass. The greatest demand of potassium is in fertilizers. Many other potassium salts are of great importance including carbonate, chloride, nitrate, bromide, sulfate and cyanide (Emsley, 2011).

Chromium (chemical symbol, Cr) is the 4^{th} transition metal found on the periodic table and has an electron configuration of [Ar] $5d^5$ $4s^1$. Cr is a hard and silvery with blue tinge. It has an atomic number of 24, located in group 6 and period 4 on the periodic table. Cr is found mainly on chromite mineral ore, found all around the world including South Africa, Turkey, etc. Cr is also used to harden steel like Na and also to manufacture stainless steel and produce several other alloys (Emsley, 2011).

Lithium vanadate (Li_3VO_4) is a compound used in a variety of fields such as electrochemistry, electronics and optics and has an orthorhombic crystal structure (Massarotti *et al*., 2005). The structure of lithium vanadate is built by corner-sharing LiO_4 and VO_4 occupying the tetrahedral sites (Zhang *et al*., 2015). The octahedral sites are vacancies and connect to establish a three dimensional (3D) channel. These empty sites exist to allow lithium-ion cation migration (Zhang *et al*., 2016).

© University of Venda

2.2 Vanadium-based electrode materials

The most frequently used cathode electrode material for lithium-ion battery (LIBs) is $LiCoO_2$ (Fergus, 2010). Because cobalt is not readily available, it is more costly when compared with other transition metals like manganese (Mn), vanadium (V), nickel (Ni), iron (Fe), and others. Even though $LiCoO_2$ is a most commonly used cathode material, other materials that are cheaper and more stable are being developed.

Chakrabarti *et al*., 2013 and Liivat *et al*., 2010 has reported that vanadate – based electrode materials have a metallic response because of the presence of vanadium states within Fermi energy. Among vanadates, Li_3VO_4, LiV_3O_8, $LiMnVO_4$, $LiNiVO_4$, $LiVO_2$, $LiVPO_4$, and $LiVTiO_4$ have been investigated for electrochemical performance. Studies of vanadate – ibased electrode materials have also been made for sodium – ion battery (Ren *et al*., 2016 and Ren *et al*., 2016).

This study, Li_3VO_4 was investigated as a promising anode material because it has interesting properties to be explored as a negative electrode. Some of the properties include, small structural and volume change during charge-discharge (lithiation and delithiation) processes, leading to a stable cyclic durability, high ionic conductivity (~10^{-4} S cm^{-1}), and maintain a high energy density (Zhang *et al*., 2016). Li_3VO_4 material has been studied for lithium-ion batteries and when discharged to 0.01 V, it showed a theoretical capacity of 591 mAh g^{-1} vs Li/Li^+ (Zhang *et al*., 2015). In 2016, Zhang doped Li_3VO_4 with nickel whiles study its effects on the structural and electrochemical behaviour of Li_3VO_4. Ni-doped LVO showed improved electrochemical performance with Ni-LVO exhibiting excellent lithium-ion storage properties with capacities of 600 mAh g^{-1} at 50 mA g^{-1}. Ni-doped LVO showed excellent capacity stability maintaining near 100 % of the initial reversible capacity after 800 cycles at 1 A g^{-1} (Zhang *et al*., 2016).

Despite the advantages mentioned above, Li_3VO_4 has its disadvantages. The main disadvantage is low electrical conductivity which may result in poor rate capability and large polarization

© University of Venda

(Zhang *et al*., 2016). For Li_3VO_4 to be considered as a negative electrode, there are key requirements that it must have. The material must

- reversibly reacts with lithium. This dictates that when lithium is added, the host structure's intercalation-type reaction does not change.
- react with lithium with a high free energy of reaction to ensure that the reaction occurs at a high voltage.
- be stable and environmentally friendly (non-toxic).
- have high electronic conductivity.
- be inexpensive to synthesize.

2.3 Improving Electrochemical Performance

Li_3VO_4 suffers from a poor electrical conductivity affecting the electrochemical behaviour, that is, poor rate capability (Liao *et al*., 2017), different ways that can be used to improve the electrode performance. Some of the ways include doping the electrode with metal ions, combining the electrode material with an electronically conductive material (like graphene, carbon nanotubes, etc.), combining two electrode materials, electrode coating, controlling morphologies of particles and many others (Ni *et al.*, 2014; Zhang *et al.*, 2016; Shi *et al.*, 2013 and Li *et al.*, 2014).

2.3.1 Forming composite with graphene

Graphene (G) has a very high electronic conductivity and it is one of the most used materials to form composites (Prabakar *et al.*, 2013; Zhen *et al.*, 2013). G possesses an ideal structure for fast lithium performance which is the two-dimensional (2D) nanoribbons or nanosheets. These structures provide a high active surface area, short Li^+ ion diffusion path, and low resistance to volume expansion when compared with bulk materials (Rui, 2013). To enhance the low electronic conductivity of Li_3VO_4, researchers started to investigate the composite of lithium vanadate (Li_3VO_4) with graphene (Jian *et al.*, 2015; Liu *et al.*, 2015; Ni *et al.*, 2015). Hollow Li_3VO_4/G composite structure was synthesized using an *in situ* one-step hydrothermal method. It was reported that the hollow Li_3VO_4/ graphene (LVO/G) composite structure shortened the ion-diffusion length while the graphene effectively enabled electron transfer (Shi

© University of Venda

et al., 2013). This composite resulted in superior rate performance and good cycle performance. However, the synthesis process was tedious.

Jian *et al.* (2015) successfully used sol-gel method to synthesize Li_3VO_4 nanoparticles embedded in graphene nanosheets (LVO@GNS). LVO@GNS composite presents excellent long-life performance with a capacity retention rate of 63.1% after 5000 cycles at 5C and high-rate performance with a stable capacity of 133 mAh g^{-1}. The XRD pattern for this composite was indexed to an orthorhombic structure (Jian., 2015).

The preparation of ultrathin Li_3VO_4 nanoribbon@graphene sandwich-like nanostructures (LVO/G) was achieved by Liu *et al.* (2015). These LVO@G sandwich-like nanostructures were prepared using the layer-by-layer assembly method. Not only did LVO@G showed excellent cycling performance, but it also showed high specific reversible capacitance of up to 452.5 mAh g^{-1} after 200 cycles. The nanostructures also showed very high rate capability.

This strategy of using ‘’graphene-like’’ binary inorganic nanosheets as templates to synthesize lithium-containing ternary oxide nanosheets, may be used to synthesize other ternary oxides having ‘’graphene-like’’ nanostructures (Liu *et al.*, 2015).

Furthermore, Mo *et al.* reported that nitrogen (N) doping can effectively enhance the capacity contribution of graphene in the composite (Mo *et al.*, 2017). Li_3VO_4/N-doped graphene (LVO/N-G) was successfully synthesized via hydrothermal pre-treatment and subsequent sintering (Ni *et al.*, 2015). This electrode material showed superior electrochemical performance with increased lithium-ion diffusion and electron transfer efficiency. After 100 cycles at a specific current of 0.15 A g^{-1}, it delivered discharge and charge capacities of 478 and 476 mAh g^{-1}, respectively.

© University of Venda

2.3.2 Forming composite with other carbon materials

The electrochemical performance of Li_3VO_4 is improved by forming composite with other carbon materials (Mo *et al.*, 2017). The most common way is to coat the surface of LVO with a uniform layer of carbon. Carbon coating is utilized to protect the electrode from direct contact with the electrolyte, enhance electrode conductivity, and improve surface chemistry of the active material. And together with nanotechnology, carbon coating provides fast lithium-ion diffusion and good conductivity resulting in improved electrochemical performance (Li *et al.*, 2012).

Shao *et al.* (2015) and Zhang *et al.* (2015) synthesized carbon-coated LVO with improved electrochemical performance because carbon coating could enhance the electrochemical performance of the composite. The enhanced electronic conductivity protects the electrode material from corrosion and dissolution in the electrolyte during the charge/discharge processes. Carbon coating could also decrease the side reactions at the electrode/electrolyte interface. For instance, Zhang *et al.* (2015) synthesized nanostructured carbon-coated LVO using a one-step solid-state reaction which presented high rate capability and long cyclic performance. The LVO/C composite maintained 80% retention after 2000 cycles at 10 C.

Furthermore, Zhang *et al.* (2016) reported on the effect of the nitrogen-doped carbon layer. Li_3VO_4/N-doped C was successfully synthesized using a solution based method which presented long cycle life and ultrahigh capacity. The charge and discharge capacities were maintained at 337 and 340 mAh g^{-1} after 1100 cycles at a specific current of 2.0 A g^{-1}.

Li *et al.* (2014) synthesized hollow Li_3VO_4/carbon nanotubes (LVO/CNTs) composite via a fast, high yield, and simple hydrothermal method. The CNTs are connected to construct a three dimensional (3D) conducting network. They bind the hollow LVO together. This 3D hollow LVO/CNTs composite is effective for energy storage materials which improves the electrical conductivity and facilitate the penetration of the electrolyte (Li *et al.*, 2014). This composite shows excellent cycle performance and very high rate performance (240 mAh g^{-1}) (Li *et al.*, 2014).

© University of Venda

Qin *et al*. (2017) reported on the one-pot synthesis of Li_3VO_4/carbon (LVO/C) nanofibers using electrospinning method. The prepared LVO/C nanofibers exhibited a unique structure whereby the nanosized LVO particles are uniformly embedded in an amorphous carbon matrix. These nanofibers showed an enhanced reversible capacity of 451 mAh g^{-1} at 40 mA g^{-1}. After 100 cycles, the capacity remained at 394 mAh g^{-1}. LVO/C nanofibers displayed stable electrode/electrolyte interface, high reactivity, and enhanced electronic conductivity.

Yan *et al*. (2020) prepared a novel Li_3VO_4/Carbon sheets (LVO/CS) composites from cellulose using simple freeze-drying and hydrothermal methods as a high-performance anode material for LIBs. XRD, FESEM, FTIR, and other techniques were used for the microstructure and elemental composition of the LVO/CS composites. The battery testing system and electrochemical workstation were used to study the electrochemical performances of the composites. The LVO/CS 2.0 (mass ration of LVO: CS was 24:1) composites exhibited excellent performance with specific capacity reaching up to 716 mAh g^{-1} after 100 cycles at low current density 0.1A g^{-1}. LVO/CS resulted in specific capacity much better than those of LVO matrix materials like LVO/carbon nanofibers, LVO/carbon nanotubes, and LVO/N-doped graphene (Yan *et al.*, 2020).

2.3.3 Doping with foreign atoms

The physical and chemical surroundings of the host lattice can be varied by introducing foreign atoms. Electrochemical performance can be directly influenced by introducing foreign atoms (Liu *et al.*, 2016). Introduction of foreign atoms, that is, doping is an effective way of improving the cycling performance or rate capability in electrode materials.

Other materials with high conductivity besides carbon are copper, nickel, and nickel oxide (NiO). These materials are reported to form composites with Li_3VO_4 to improve the conductivity and they exhibited better capacity and rate capability. Ni *et al.*, (2014) reported on the fabrication of Li_3VO_4/Ni. Though nickel served as a current collector, it also improved the conductivity of lithium vanadium tetroxide resulting in improved electrochemical performance. Zhang *et al.*, (2016) also introduced nickel into Li_3VO_4 to investigate nickel's effects on the structure and electrochemical performance of Li_3VO_4. The results showed that

© University of Venda

nickel doped Li_3VO_4 exhibited a capacity of 650 mA g^{-1} at 50 mA g^{-1} and high surface energy. This material was able to supply almost 100% capacity retention after 800 cycles at 1 A g^{-1} (Zhang *et al*., 2016).

Copper-doped Li_3VO_4 was prepared by a simple and inexpensive sol-gel method. The doped Li_3VO_4 delivered high initial discharge and charge capacities of up to 63 mAh g^{-1} after 25 cycles for 5 % Cu-doped material at a rate of 0.5 C. Conductive Cu was found to enable better Li^+ ion storage due to the improved electronic conductivity, Li ion diffusion, and structural stability, improving cycling and rate performance (Mulaudzi *et al*., 2020).

Reducing the particle size of the electrode material can also improve the performance (Ni *et al*., 2015). Considering Li_3VO_4 (LVO), the lithium ion-diffusion has an important effect on the electrochemical performance of LVO. This shows a close relationship with the size of LVO particles. The smaller the particle size of LVO is, the higher the lithium ion-diffusion efficiency will be (Ni *et al*., 2015). Previous study shows that solution-based methods like hydrothermal, solution precipitation, and sol-gel method are effective in reducing the size of LVO (Ni *et al*., 2015).

Li_3VO_4 has been used to coat $Li_{1.18}Co_{0.15}Ni_{0.15}Mn_{0.52}O_2$ cathode material. Fu *et al*., (2014) found that LVO surface coating improved the activation of manganese ions, hence resulting in a high discharge capacity. Li_3VO_4 also prevented solid electrolyte interface (SEI) film growth and improved the cycle stability & rate capability of the electrode material. LVO as a coat for $Li_{1.18}Co_{0.15}Ni_{0.15}Mn_{0.52}O_2$ improved the thermal stability of material (Fu *et al*., 2014).

© University of Venda

Chapter 3: Research Methodology

This chapter outlines the experimental procedures and techniques that were used for the preparation and analysis of the lithium vanadate samples (undoped and doped). The samples were prepared using the citrate sol-gel method. Subsequently, the characterization techniques used to analyze the structure of undoped and doped (with Na, K, Cr) was discussed. X-ray diffraction (XRD) was used to investigate the identity and crystallinity of the prepared lithium vanadate samples. Elemental composition and functional groups were determined by energy-dispersive X-ray spectroscopy (EDS) and Fourier transform infrared spectroscopy (FTIR).

3.1 List of chemicals

The chemicals that are used in the study are listed in Table 3.1 below.

Table 3.1: List of chemicals and their chemical formula, purity, molar mass and purpose

List of chemicals	Chemical formula	Purity (%)	Molar mass	Purpose
Lithium nitrate	$LiNO_3$		68.95	Source of Li-ion
Vanadium oxide	V_2O_5	99	181.88	Source of V-ion
Citric acid	$C_6H_8O_7 \cdot H_2O$	99.8	210.14	Chelating agent
Sodium carbonate decahydrate	$Na_2CO_3 \cdot 10H_2O$	99	286.14	Source of Na-ion
Potassium carbonate anhydrous	K_2CO_3	99.8	138.21	Source of K-ion
Chromium oxide	Cr_2O_3	98	151.99	Source of Cr-ion

3.2 Experimental procedures

To study the structural and electrochemical performance of Li_3VO_4, $Li_{3-x}Na_xVO_4$, $Li_{3-x}K_xVO_4$, $LiV_{1-y}Cr_yO_4$, and $Li_{3-x}K_xV_{1-y}Cr_yVO_4$ (where x = 0.01, 0.05 & 0.1M; y = 0.01, 0.05 & 0.1M) anode materials, citrate sol-gel method, summarized in Figure 3.1, was used. The stepwise synthesis procedures and the synthesis technique are discussed below:

© University of Venda

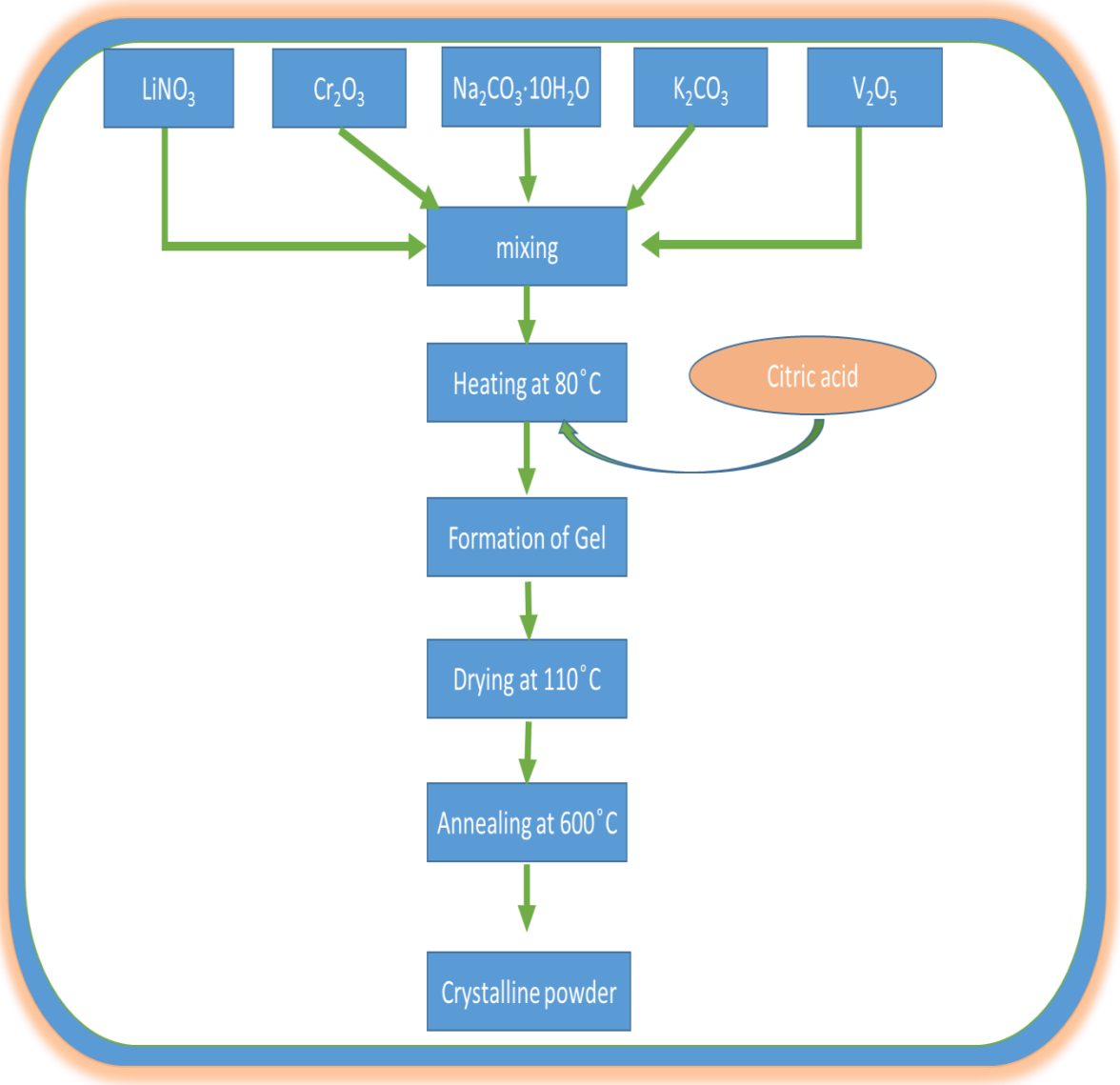

Figure 3.1: Flow chart for the synthesis of undoped and doped lithium vanadate by sol-gel method

3.2.1 Powder preparation

To study the structural and electrochemical performance of Li_3VO_4, $Li_{3-x}Na_xVO_4$, $Li_{3-x}K_xVO_4$, $LiV_{1-y}Cr_yO_4$, and $Li_{3-x}K_xV_{1-y}Cr_yVO_4$ (where x = 0.01, 0.05 & 0.1M; y = 0.01, 0.05 & 0.1M) anode materials samples were synthesized in the form of powder by citrate sol-gel method.

© University of Venda

For the host (Li_3VO_4), stoichiometric amounts of lithium nitrate and vanadium oxide were dissolved in 30 mL distilled water under magnetic stirring at room temperature for 30 minutes. Singly-doped $Li_{3-x}Na_xVO_4$, $Li_{3-x}K_xVO_4$, and $LiV_{1-y}Cr_yO_4$ were synthesized by dissolving stoichiometric amounts of lithium nitrate, vanadium pentoxide, and either sodium carbonate decahydrate, potassium carbonate anhydrous or chromium oxide in 30 mL of distilled water. For co-doped $Li_{3-x}K_xV_{1-y}Cr_yVO_4$, stoichiometric amounts of lithium nitrate, vanadium pentoxide, potassium carbonate anhydrous and chromium oxide were dissolved in 30 mL distilled water at room temperature for 30 minutes. The solutions were heated at 80 ^oC and citric acid (3M) was added into the solutions dropwise with continuous stirring until all the excess water was removed to form a foam. The foam was dried in an oven at 110 ^oC overnight. The dried foam was ground using pestle and mortar and annealed at 600 ^oC for 3 hours in a furnace.

3.3 Synthesis method

The easiness of fabricating the desired compound and controlling certain factors like particle shape and size are key to the growth of nanoscience and nanotechnology. This was accomplished by years of development of different synthesizing techniques, like citrate sol-gel, solid-state reaction, hydrothermal, co-precipitation, etc. These methods also give products with better electrochemical performances (Zhang, 2015). In this study, the citrate sol-gel method was used to synthesize lithium vanadate doped with alkali metals (Na, K) and transition metal (Cr). Citrate sol-gel is one of the most versatile and attractive methods because it produces pure and ultrafine powders at a very low temperature (Zhang. 2015). There are different methods for synthesizing electrode materials as indicated above.

3.3.1 Citrate sol-gel method

Currently, the sol-gel method has become a convenient route to synthesize nanoparticles utilizing different precursors. Sol-gel is typically used to produce nano-sized particles, mostly metal oxides. This method has proved to be economical, flexible, and less complex when compared to conventional routes. Sol-gel has been extensively utilized in the field of glass, thin film-coatings, and ceramics (Zhang, 2015).

© University of Venda

Sol-gel method is preferred because of various advantages over the conventional solid-state reactions such as short heating time, good crystallinity, homogeneous mixing at the atomic or molecular level, low synthesis temperature, good stoichiometric control, uniform particle size, and small diameter (Liu *et al.*, 2004 and Zhang, 2015). This method can be dated back to as early as 1846 when Ebelenen discovered the formation of SiO_2 gel by hydrolyzing $Si(OEt)_4$ (Liu *et al.*, 2004). Further development of sol-gel method began in the 1930s (Liu *et al*., 2004).

Although the advantages of the sol-gel method have been described above, the shortcomings are also obvious:

1. Addition of organic compounds increases the costs,
2. The utilization of a reactor is lower due to the expansion of the gas, and
3. During the annealing or calcination process, grain growth may occur.

The first step of this method is to convert the starting material (monomers) into a sol, that is, a colloidal solution (precursor) for further formation of a gel. The gel is made up of polymers (discrete particles). The precursors are hydrolyzed and then polycondensed for the formation of colloids. The low temperature and economical flexibility gives the control over the composition of the synthezised products (Song *et al*., 2002). Furthermore, small amounts of dopants like transition metals, rare earth metals, and organic dyes can be used in the sol which disseminates homogeneously in the formed products. The synthesized products can be utilized in the processing and manufacturing of ceramics. Synthezised materials from the sol-gel method have a wide area of application in energy, optics, medicine, space, reactive materials, etc (Liu *et al.*, 2004; Agrawal *et al.*, 2011 and Dickson *et al.*, 2013).

In recent studies, researchers have reported lithium vanadate materials synthesized by the sol-gel method in the presence of citric acid (CA). This method is now known as citrate sol-gel or citric sol-gel. The addition of citric acid to the traditional sol-gel method has added the following advantages:

1. Serves as a chelating agent,

© University of Venda

2. Stabilizes the sol-gel method,
3. Adjusts the pH, and
4. Increases the magnitude of zeta potential of particle surface modifier.

In this study, the citrate sol-gel method was used to synthesize Li_3VO_4 doped (with Na; K and/or Cr).

The basic processing steps involved in sol-gel can be summarized as follows:

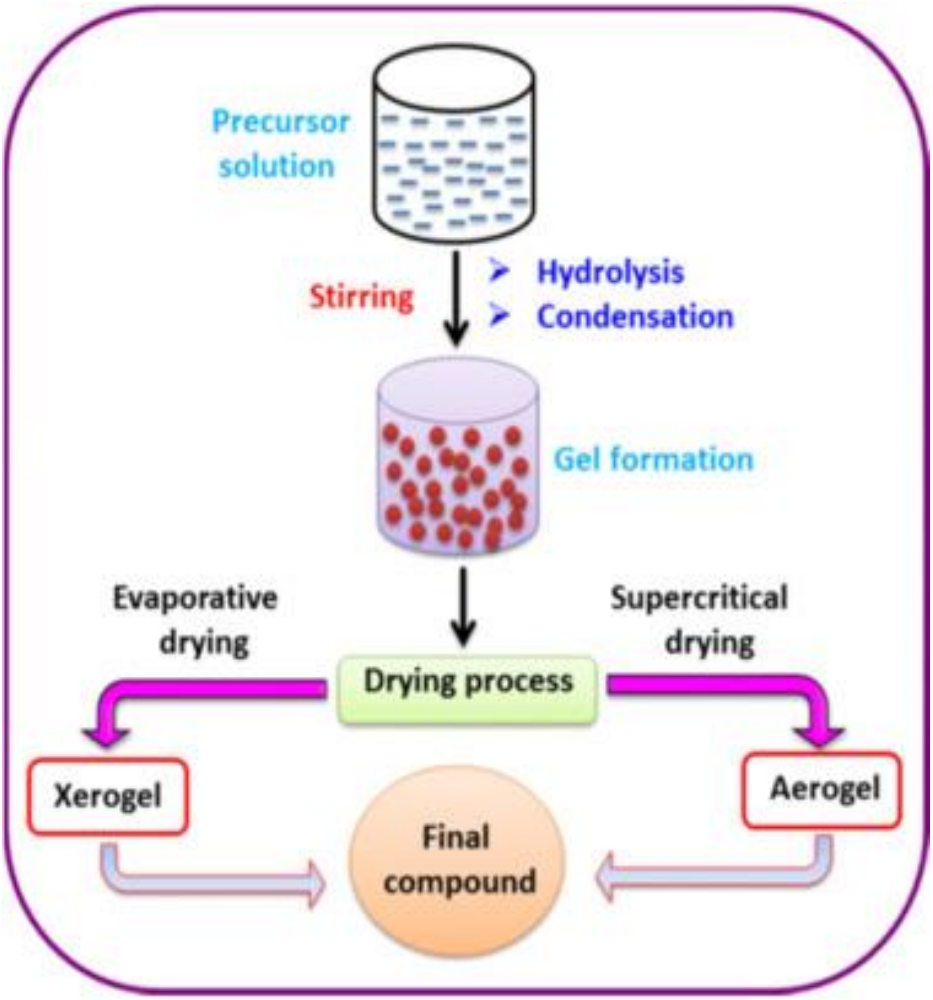

Figure 3.2: The reaction pathway for the production of metal oxide nanostructures by sol-gel method (Rao *et al.*, 2017)

© University of Venda

3.4 Characterization Techniques

3.4.1 X-ray diffraction spectroscopy (XRD)

Powder X-ray diffraction spectroscopy (XRD) is a non-destructive technique mostly used for the characterization of crystalline materials. The structural properties of the doped and un-doped Li_3VO_4 were studied using the X-ray diffraction spectroscopy. This technique was applied to provide information on the phase, crystal size, lattice parameter, degree of crystallinity, inter-planar spacing (d-spacing), strain, and the crystal orientation (Bunaciu *et al.*, 2015). The physical states of the materials to be analyzed can be thin films, loose powders, polycrystalline and bulk materials. The phase and lattice parameter help to confirm the expected crystalline nano-material by comparing with the known lattice parameter and diffraction patterns of inorganic compound available in the Powder Diffraction Files (PDF) of the International Centre for Diffraction Data (ICDD) and Joint Committee on Powder Diffraction Standards (JCPDS) (Cao, 2004).

Crystalline materials act as 3D diffraction gratings, for X-ray wavelength, similar to the spacing of planes in a crystal lattice. The X-ray diffractometer consists of three basic components, which are: X-ray tube, sample holder, and X-ray detector (Bunaciu *et al.*, 2015). A cathode-ray tube generates X-rays that are filtered to produce monochromatic radiation. When monochromatic radiations are directed towards the sample, constructive interference (and diffracted rays) are produced when conditions satisfy Bragg's Law:

$$2d \sin\theta = n\lambda \quad \ldots (3.1)$$

where d is the inter-planar spacing (nm)

n is the order of reflection

λ is the radiation wavelength (CuK_α = 0.15406 nm)

θ is the angle of diffraction (degrees)

Bragg's equation (3.1) can be used to calculate the inter-planar spacing (d-spacing) of the planes. The Bragg's law relates the wavelength of electromagnetic radiation to the diffraction angle and the lattice spacing in a crystalline sample. The diffracted rays are detected, processed,

© University of Venda

and counted. By scanning the sample through a range of 2θ angles, all possible diffraction directions of the lattice are attained because of the random orientation of the powdered material. The identification of the mineral can be done by converting diffraction peaks to d-spacings since each mineral has a set of unique d-spacings. Typically, the d-spacings are compared with the standard reference patterns (Bunaciu *et al.*, 2015).

For diffraction to happen, λ must not be greater than twice the inter-planar spacing. The inter-planar spacing and the lattice parameters are related to the miller indices (*hkl*) of each plane. The crystallite size of the nanomaterial can be calculated by the Scherrer's equation (3.2) (Maphiri *et al.*, 2017):

$$D = \frac{k\lambda}{\beta \cos\theta} \quad \ldots (3.2)$$

where D is the crystallite size

β is the full width at half maximum (FWHM) of an XRD diffraction peaks

k is the Scherrer's constant

λ is the radiation wavelength (CuK_α = 0.15418 nm)

θ diffraction angle

In this study, the crystalline phase of the prepared sample was identified by powder X-ray diffraction (PXRD) using Cu Kα radiation (λ = 1.54184). The samples were sprinkled on the silicon XRD sample holder and placed inside the machine. The measurement was done at angle of 2θ = 10° to 90°.

3.4.2 SEM-EDS

The scanning electron microscopy (SEM) was used to study the topography and morphology of the un-doped and doped Li_3VO_4 (using Na, K, Cr) by capturing the micrograph (image) of the sample's surface. The SEM technique operates according to the following basis: The electron beam is emitted from an electron gun and accelerated towards the surface of the sample. The electron beam is focused by condenser lenses into a beam with a thin spot size.

© University of Venda

Then passes through the objective lens, where is deflected linearly or raster fashion by a pair of coils over a rectangular area of the sample surface (Goldstein *et al*., 2017 and Akhtar *et al*., 2018). In general, the SEM micrograph is captured by focusing an electron beam across the sample while detecting the secondary electron intensity as a function of the primary beam position to build up the micrograph (Schroder., 2006). Non-metallic sample such as ceramics and organic material requires carbon (C) or gold (Au) coating before being studied. Metal samples are conductive and do not require coating. The non-metallic sample coating process is done by using a sputter coater.

The Energy dispersive X-ray spectroscopy (EDS) functions on a similar basis as SEM. The difference is that the EDS monitors the backscattered electrons and characteristic X-rays. The detector converts the backscattered electrons into an EDS image. The EDS spectrum is a result of counting characteristic X-rays corresponding to certain energy levels within the sample.

In this research, the size and surface morphology of the powder materials were examined by a scanning electron microscope (SEM) using Zeiss Crossbeam 540 FEG SEM. The elemental composition of the sample was characterized by energy-dispersive X-ray spectroscopy (EDS) using Aztec 30 SP1 software. Samples were sprinkled on the sample holder covered with carbon tape. The sample holder with the sample was carbon coated (This increased the sample conductivity). The sample was placed inside SEM, which was done at 2 Kv and the EDS was done at 20 Kv.

3.4.3 Fourier Transform infrared spectroscopy (FT-IR)

The most powerful technique used in the analytical laboratories is infrared spectroscopy which is associated with the infrared region. There are a variety of compounds either inorganic or organic which are absorbed at various frequencies of electromagnetic radiation. Fourier transform infrared spectroscopy can be employed for a long-range of frequencies varying over ultraviolet, visible, near-infrared, mid-infrared, and even far-infrared regions by selecting different beam splitters and detectors for the required ranges (Jaggi *et al.*, 2006).

© University of Venda

IR spectroscopy is useful in determining chemical structure because the energy that corresponds to specific values allows us to identify various functional groups within a molecule. A mid-IR spectrum usually extends from radiation around 4000 cm^{-1} to 400 cm^{-1} and can be split into the functional group region and the fingerprint region. The fingerprint region is different for each molecule just like a fingerprint is different for each person.

There are several instruments used in determining the absorption for a compound and an example of such an instrument is known as an infrared spectrometer. There are two kinds of infrared spectrometer, namely: dispersive infrared spectrometer and Fourier transform infrared spectrometer (FT-IR). They both measure the spectra of the compounds in the range of 4000 cm^{-1} to 400 cm^{-1}. Nowadays, different industries and laboratories prefer to use the FT-IR spectroscopy because it gives infrared spectrum within a second and the FT-IR spectroscopy does not have slits where some of the light can pass through (UKEssays, 2018). The FT-IR spectroscopy has three main components which are radiation source, interferometer, and detector.

The main advantage of an FT-IR spectroscopy is that it collects many interferograms of the sample and store them in a computer memory. To obtain a spectrum of the sample, the person analyzing (chemist, physicist, material scientist, etc.) must first obtain an interferogram of the background which consists of the infrared-active atmospheric gases, water vapor, and carbon dioxide. The interferogram is subjected to a Fourier transform (which yields the background spectrum). Then the sample is placed and the spectrum is obtained resulting from the Fourier Transform of the interferogram. The spectrum obtained contains absorption bans for both the background and the sample (UKEssays, 2018). The computer software automatically subtracts the background spectrum from the spectrum of the sample being analyzed.

In the present study, the alpha Fourier transform infrared (FTIR) spectrometer (Bruker optics 7.0) equipped with alpha platinum was used to characterize the functional groups of the prepared samples. The samples were placed on the alpha platinum and the measurement was done using transmittance method in the wave number region of 400 cm^{-1} – 4000 cm^{-1}. Before each measurement is done, the FTIR spectrometer is run with no sample added in order to

© University of Venda

establish the background measurement, which is then automatically subtracted from the sample spectrum. This help in elimination of instrument influence during measurement.

3.4.4 Raman Spectroscopy (RS)

Raman spectroscopy (RS) has been a field of major advances since the discovery of the Raman effect in 1928 by Sir Raman C.V. who was awarded the 1930 Nobel prize in physics. Due to the unavailability of intense monochromatic light sources and the lack of suitable optical components and detectors, RS was primarily used to study vibration states of simple molecules. Raman spectroscopy has been increasingly applied to solve problems of both fundamental and technological interest since the discovery of lasers in the 1960s and the development of high-throughput monochromators and sensitive detectors (Atalla *et al.*, 2012). Raman spectroscopy is a technique based on inelastic scattering of monochromatic light, usually from a laser source, through its interaction with vibrating molecules. It probes molecular vibrations (Bumbrah *et al.*, 2016).

Raman spectroscopy is a versatile method that is used for analyzing a wide range of molecules and minerals. It also has important scientific applications in studying molecular structures. Raman spectroscopy resolves most of the limitations of other spectroscopic methods and can be used for both qualitative and quantitative analysis (Skoog *et al.*, 2017). Qualitative analysis can be performed by measuring the frequency of scattered radiations whereas quantitative analysis can be done by measuring the intensity of scattered radiations (Skoog *et al.*, 2017).

When light interacts with molecules in a solid, liquid, or gas, the vast majority of the photons are scattered or dispersed at the same energy as the incident photons. This is elastic scattering (or Rayleigh scattering). A small number of photons scatter at a different frequency than the incident photon. This is described as inelastic scattering (or Raman effects). As described by quantum mechanics, Raman scattering is that when photons interact with a molecule, the molecule may be advanced to a higher energy. From this higher energy state, different outcomes may occur. One outcome may be that the molecule relaxes to a vibrational energy level that is different than the one of its beginning state and this produces a photon of different energy. The difference in the energy of the incident photon and the energy of the scattered

© University of Venda

photon is known as the Raman shift (Bumbrah *et al.*, 2016). When the change in energy of the scattered photon is less than the incident photon, the scattering is known as Strokes scatter. Some molecules may start in a vibrationally excited state and when they are advanced to the higher energy state, they may relax to a final energy state that is lower than the initial excited state. This is known as anti-strokes (Bumbrah *et al*, 2016).

A typical conventional Raman system consists of four basic components, namely:

- An excitation source, (mostly used is visible-light laser)
- Optics for sample illumination and collection of sample scattered light
- A monochromator
- A signal processing system having a detector and a data processing unit.

In this work, Raman optical microscope, WItec, was used to record Raman spectrum of the sample in the wavenumber region of interest 100–1500 cm^{-1}. The samples were placed on the microscopic glass substrate and place under the 100x Nikon objective and focused. The measurement was done at 2 milliwatts (mW) using the 532 nm laser at the integration time of 30s and accumulation of 4.

© University of Venda

4.1.1 Powder X-ray diffraction spectroscopy

The phase analysis was carried out on the prepared product by using powder X-ray diffraction (XRD) technique. The prepared product, that is, Li_3VO_4 (LVO) was annealed at 600 °C for 3 hours to eliminate nitrogen dioxide (NO_2). Figure 4.1 exhibits the XRD pattern of Li_3VO_4 prepared via the citrate sol-gel method. The pattern obtained for the prepared LVO exhibits sharp peaks indicating the high order of crystallinity. As seen from diffraction peaks located at 16.5°, 21.9°, 23.1°, 24.4°, 28.5°, 33.0°, 36.6°, 37.9°, 50.1°, 58.8°, 66.5°, and 71.0° can be attributed to the (100), (110), (011), (101), (111), (200), (002), (201), (202), (320), (203) and (322) crystal faces of orthorhombic LVO of space group, Pmn21. The lattice parameters (a = 6.33138 Å, b = 5.45077 Å and c = 4.95167 Å) were calculated by Rietveld refinement using Fullprof software and the above results are in well agreement with the literature (Ni *et al.*, 2014).

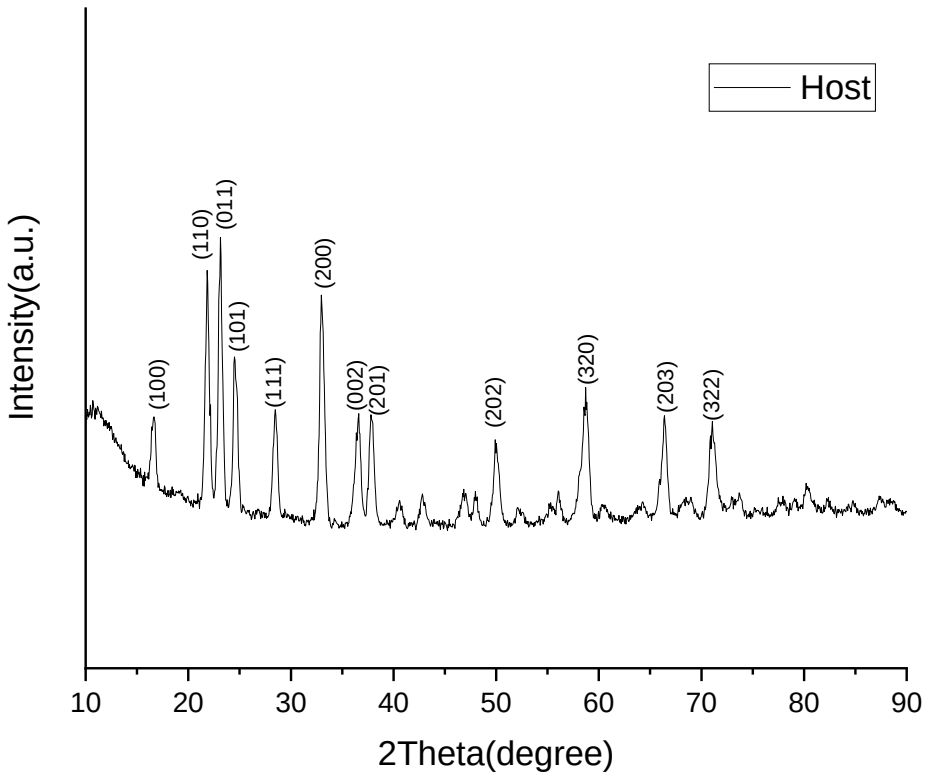

Figure 4.1: XRD pattern of Li_3VO_4 (host) annealed at 600 ℃ for 3 hrs

© University of Venda

It can be seen that the prepared materials (undoped, singly and co-doped) are fully crystalline and the diffraction peaks could be indexed to the orthorhombic single phase of Li_3VO_4 (PDF: 38-1247) with space group Pmn21.

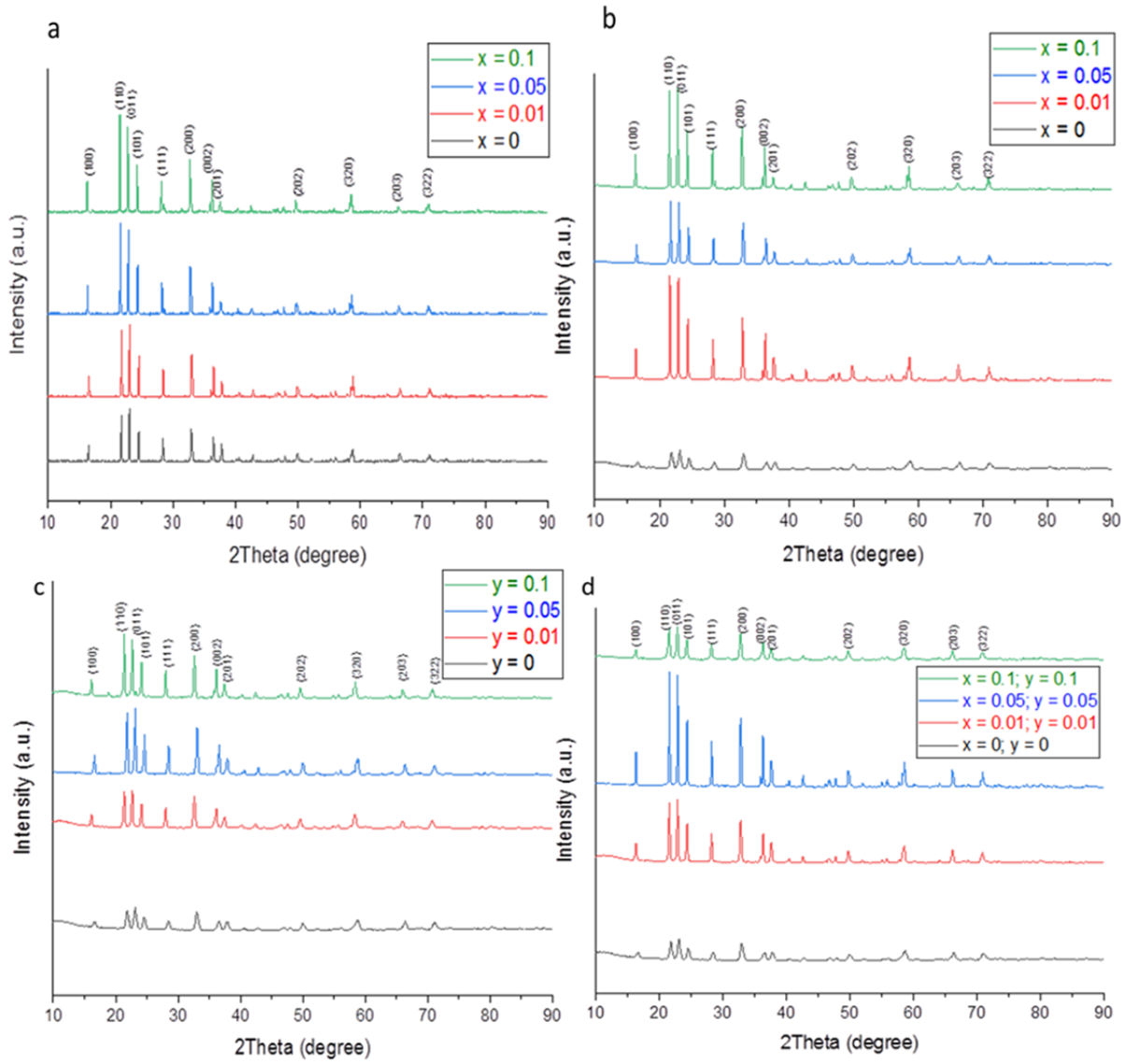

Figure 4.2: XRD pattern of (a) $Li_{3-x}Na_xVO_4$ (b) $Li_{3-x}K_xVO_4$ (c) $Li_3V_{1-y}Cr_yO_4$ and (d) $Li_{3-x}K_xV_{1-y}Cr_yO_4$ (doped at x = 0, 0.01, 0.05, 0.1 and y = 0, 0.01, 0.05, 0.1) annealed at 600 ℃ for 3 hrs

XRD patterns of the $Li_{3-x}Na_xVO_4$ (x = 0, 0.01, 0.05 and 0.1) powders are shown by Figure 4.2a. The diffraction peaks of all the prepared samples were in good agreement with the standard

© University of Venda

diffraction peaks of Li_3VO_4. The peaks were indexed to an orthorhombic crystal structure with a space group of Pmn21. No obvious impurity peaks are detected. Sodium-doped samples have much stronger peak intensity than that of the host sample LVO, especially for the x = 0.05 and 0.1 samples. This indicates that sodium-doping can improve the crystallization of the material.

Na-doping on the lattice can clearly be seen by the magnified (200) peaks of $Li_{3-x}Na_xVO_4$ (x = 0, 0.01, 0.05, and 0.1) samples plotted in Figure 4.3. The (200) peaks gradually shift to a lower angle position as doping content (x) increases from 0 to 0.1. This shift suggests that the Na-doped samples have an expanded lattice compared to the host LVO. To describe the structural change induced by doping LVO with sodium, a Rietveld refinement was conducted on the XRD patterns for the prepared samples and the results are shown in Table 4.1.

Table 4.1 shows the obtained lattice parameters. It can clearly be seen that the lattice parameters *a, b, c* increases with increasing sodium-doping content. This may be ascribed to the larger ionic radius of Na^+ (0.97 Å) dopant than the Li^+ (0.68Å), suggesting the successful incorporation of sodium into the LVO crystal structure. The slight increase in lattice parameters *a, b, c* may also suggest that the sodium dopant does not change the structural characterization of Li_3VO_4.

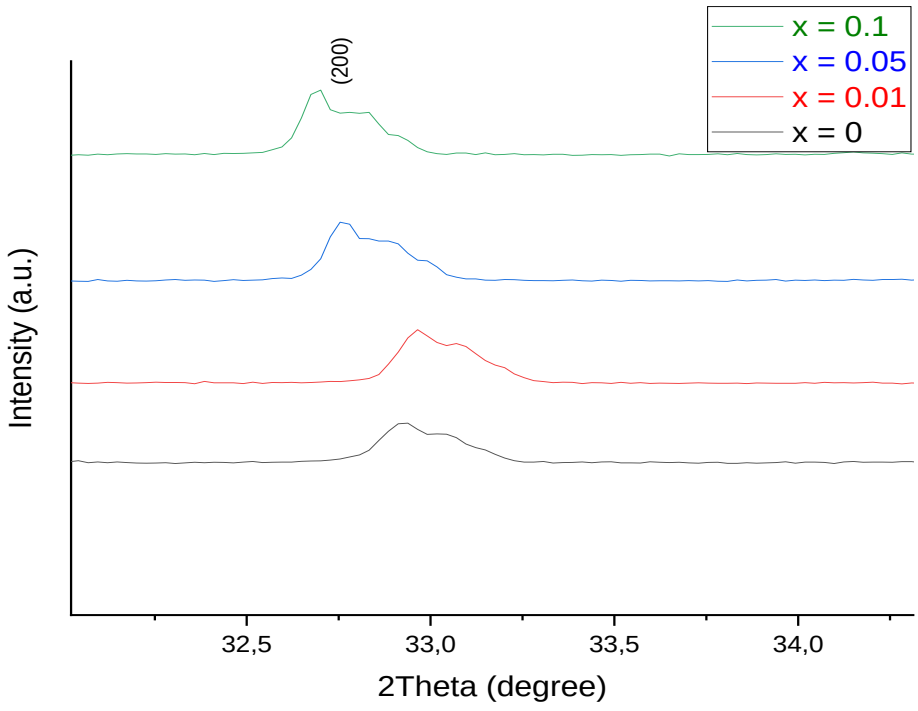

© University of Venda

Figure 4.3: Analysis of diffraction peak shift at (200) for $Li_{3-x}Na_xVO_4$ doped at x = 0.01, 0.05 and 0.1

Table 4.1: Calculated lattice parameters for $Li_{3-x}Na_xVO_4$ (x = 0, 0.01, 0.05 and 0.1) samples, based on XRD data refinement

Sample	*a* (Å)	*b* (Å)	*c* (Å)
0	6.331	5.451	4.952
0.01	6.334	5.452	4.953
0.05	6.343	5.455	4.954
0.1	6.354	5.459	4.961

Figure 4.2b shows the XRD pattern of $Li_{3-x}K_xVO_4$ (x = 0, 0.01, 0.05, and 0.1) synthesized by citrate sol-gel method, and the results are in good agreement with the standard JCPDS Card No. 38-1247. All diffraction peaks confirmed the high crystalline nature and indexed to the orthorhombic crystal structure with the Pmn21 space group. The Bragg's angle at 16.5°, 21.9°, 23.1°, 24.4°, 28.5°, 33.0°, 36.6°, 37.9°, 50.1°, 58.8°, 66.5° and 71.0° corresponds to (100), (110), (011), (101), (111), (200), (002), (201), (202), (320), (203) and (322) planes, respectively. Rietveld refinement was conducted on the XRD patterns for the prepared samples. The structural changes (lattice parameters *a*, *b*, *c*) induced by potassium doping of Li_3VO_4 are shown in Table 4.2. Table 4.2 shows the obtained lattice parameters (*a*, *b*, *c*) as concentration of K was varied. The main reason why K^+ occupies the Li-site rather than the Vanadium site is because of different ionic radius and ionic valence state. The ionic radius of K^+ and Li^+ are 1.33 Å and 0.68 Å, respectively. There is significantly smaller difference between ionic radius of K and Li-ion. Additionally, the valence state between V^{5+} and K^+ is significantly larger as compared to that of Li^+ and K^+. Therefore, K^+ occupied the lithium site more easily for the formation of single phase and stable LVO. However, a varying of lattice parameters can be seen in Table 4.2 and this is due to the slightly different ionic radius of Li^+ and K^+.

© University of Venda

Table 4.2: The lattice parameters of $Li_{3-x}K_xVO_4$ ($0 \leq x \leq 0.1$) obtained from Rietveld refinement

Sample	*a* (Å)	*b* (Å)	*c* (Å)
0	6.331	5.451	4.952
0.01	6.333	5.454	4.953
0.05	6.333	5.456	4.955
0.1	6.337	5.460	4.956

Figure 4.2c shows the XRD patterns of the prepared $Li_3V_{1-y}Cr_yO_4$ ($0 \leq y \leq 0.1$). sharp diffraction peaks located at 16.5°, 21.9°, 23.1°, 24.4°, 28.5°, 33.0°, 36.6°, 37.9°, 50.1°, 58.8°, 66.5°, and 71.0° can be clearly observed, corresponding to (100), (110), (011), (101), (111), (200), (002), (201), (202), (320), (203) and (322) planes, respectively. The peaks were indexed to an orthorhombic crystal structure with space group, Pmn21. It can be seen that the chromium-doped LVO samples gave a very similar diffraction profile to that of Li_3VO_4. All diffraction peaks of the three patterns could be fully indexed into an orthorhombic crystal structure of space group, Pmn21, with the Fullprof program, and no impurities were detected in the pattern. To further explore the structural changes affected by the Cr doping, a Rietveld refinement was conducted for the prepared samples. Table 4.3 shows the lattice parameters obtained during the refinement. The derived lattice parameters have a slight increase in Cr-doped LVO from pure lithium vanadate as seen in Table 4.3 and this is due to the slightly larger ionic radius of Cr^{3+} (0.62 Å) than $V5^{+}$ (0.59 Å). Using the Debye Scherrer formula, the average grain size of the LVO was found to be 47.8 nm.

Table 4.3: The lattice parameters of $Li_3V_{1-y}Cr_yO_4$ ($0 \leq y \leq 0.1$) obtained from Rietveld refinement using Fullprof software

Sample	***a* (Å)**	***b* (Å)**	***c* (Å)**
0	6.331	5.451	4.952
0.01	6.336	5.455	4.952
0.05	6.342	5.461	4.955
0.1	6.347	5.463	4.959

© University of Venda

The XRD was applied to study the crystallinity phase of the $Li_{3-x}K_xV_{1-y}Cr_yO_4$ ($0 \leq x \leq 0.1$) sample displayed in Figure 4.2d. The XRD patterns show the narrow diffraction peaks indicating the crystalline nature of the prepared sample. The narrow profile also indicates the homogeneous distribution of cations within the structure. The XRD spectra of the doped samples are similar to those of the host spectrum, suggesting a successful substitution of K and Cr ion into the Li_3VO_4 matrix. These results also show that there are no Li, K, V, or Cr related impurities. The average crystallite size (D) was calculated from XRD patterns, using equation 3.1 (Scherrer's equation) as described in Chapter 3 of this dissertation. The Scherrer's equation has been applied to predominant XRD lines, namely (110), (011), (101), (111), and (200). The crystallite size was found at 47.53 nm.

© University of Venda

4.1.2 Fourier transform infrared spectroscopy

The FTIR spectrum of Li_3VO_4 (LVO) synthesized via the citrate sol-gel method is shown in Figure 4.4a. FTIR signature bands observed for LVO in the 400 – 800 cm^{-1} region are largely associated either with the bending vibrations of V–O–V of VO_4 tetrahedron or vibrations of LiO_6 octahedral units. The possible bonding of Li with each oxygen atom in the VO_4 tetrahedra brings about some asymmetry, but without distorting the symmetry of the fundamental unit cell. A sharp peak at around 771 cm^{-1} can be assigned to the stretching mode of the VO_4 unit. Two weak bands around 429 and 454 cm^{-1} may, therefore, be assigned to stretching of Li–O in the LiO_6 environment.

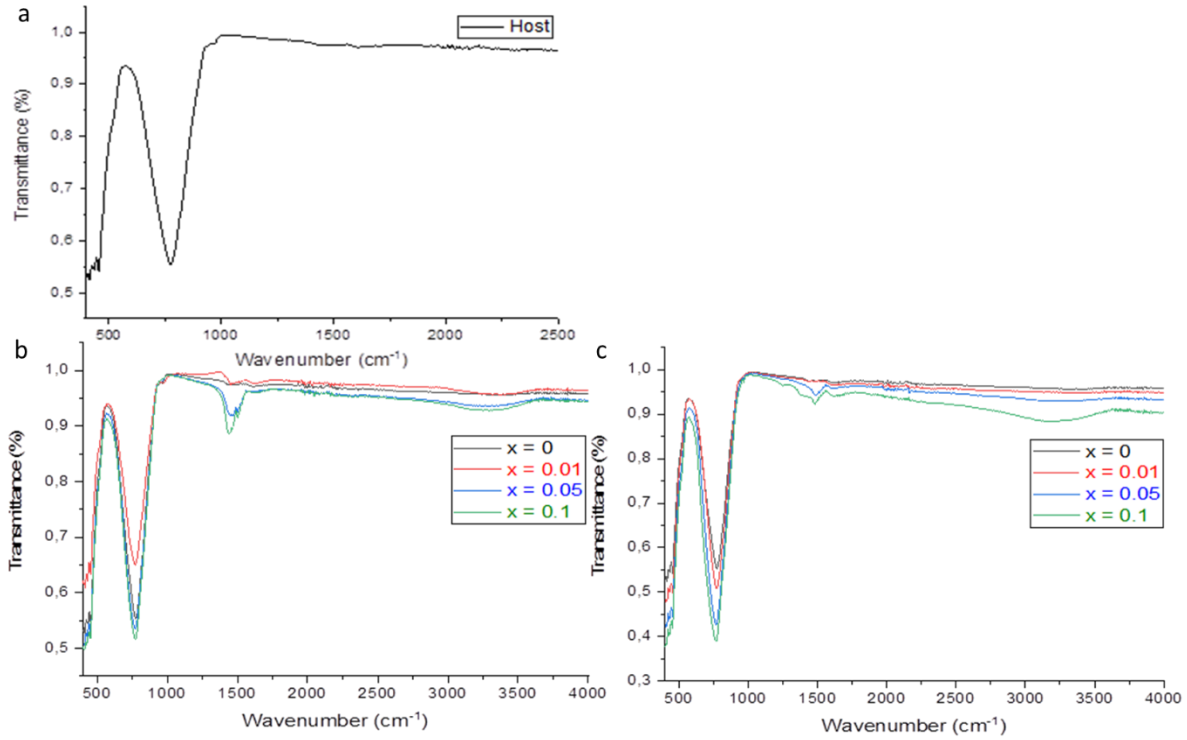

Figure 4.4: The FTIR spectrum of (a) host (b) $Li_{3-x}Na_xVO_4$ and (c) $Li_{3-x}K_xVO_4$ doped at x = 0.01, 0.05 and 0.1

Figure 4.4b shows the FTIR spectra of Li_3VO_4 (LVO) and sodium-doped LVO synthesized by the citrate sol-gel method. The FTIR peaks at around 400 – 800 cm^{-1} region, for undoped and doped LVO, are largely associated either with the bending vibration of VO_4 tetrahedron or LiO_6 octahedral units (Bhuvaneswari *et al.*, 2005). A sharp peak at around 771 cm^{-1} can be assigned to the stretching mode of the VO_4 unit.

© University of Venda

When comparing the FTIR spectra, Figure 4.9, of the host and $Li_{3-x}Na_xVO_4$ doped at x = 0.01, 0.05, and 0.1. It can be seen that as a concentration of sodium increases, the band in the region 1300 - 1500 cm^{-1} becomes narrower. This is due to the Na–O bond in the doped Li_3VO_4. For x = 0.05 and 0.1, there is a broadening of O–H peak at around 3000 – 3600 cm^{-1} and this is because the material synthesized is hygroscopic (Yang *et al*., 2020). The broad strong bands in the region 600 – 800 cm^{-1} can be assigned to a stretching vibration between the oxygen and vanadium (V=O) of the VO_4 tetrahedron.

Figure 4.4c shows the FTIR spectra of potassium doped lithium vanadate treated at 600 °C. FTIR signature peaks observed for $Li_{3-x}K_xVO_4$ ($0 \leq x \leq 0.1$) in the 600 – 1000 cm^{-1} region are largely associated with the bending vibrations of the VO_4 tetrahedron. The broad sharp peak at around 600 cm^{-1} is due to V = O vibrations. It can be seen that as the concentration of potassium increases, new peaks started to appear. The peaks at approximately 1500 cm^{-1} are due to K–O vibrations. A broad peak due to –OH bond appears at around 3000 – 3600 cm^{-1}. This O–H vibration appears because, during the IR analysis, the sample was reacting with moisture (samples are hygroscopic). Hence, the broad peak at around 3300 cm^{-1} is attributed to the moisture inside the samples (Yang *et al*., 2020).

© University of Venda

4.1.3 Raman Spectroscopy

Raman spectroscopy is very sensitive in differentiating different types of crystal symmetries whose atomic arrangements are closely related to each other (Karan *et al*., 2008 and Bowley *et al*., 2012). Despite its orthorhombic crystal structure and Pmn21 space group, the LVO Raman features can be better understood when taking into account separately the vibrations of LiO_4 tetrahedra (which give rise usually to Raman modes below 500 cm^{-1}) and the VO_4 tetrahedra group. Considering the VO_4 vibrations, we can take as a comparison $LiNiVO_4$ (cubic spinel structure, Fd3m(Oh7)) symmetry (Lai *et al*., 2001). The strongest Raman peaks, associated with the stretching vibrations, are observed at 794 and 825 cm^{-1} as for our LVO sample (Figure 4.5). The bending vibrations, responsible for the signal at 337 cm^{-1} is also present in our LVO Raman spectrum. The main Raman peak due to the band stretching and bending vibrations of V–O modes in VO_4 unit for Li_3VO_4 appear at around 794 and 825 cm^{-1}, respectively, which is in good agreement with previously reported Raman peaks of lithium vanadate (Jiang *et al*, 2017 and Yan *et al*., 2020).

In the lower energy region from Figure 4.15, several less intense Raman peaks can be observed. Raman modes are observed for the lithium vanadate at around 335, 358, 372, 386, and 459 cm^{-1}. In the 500 – 750 cm^{-1} region, no Raman peaks are present. These signals are most likely due to the couplings between some of the vibrations mentioned above.
Figure 4.3 shows the Raman spectrum of the host (lithium vanadate).

© University of Venda

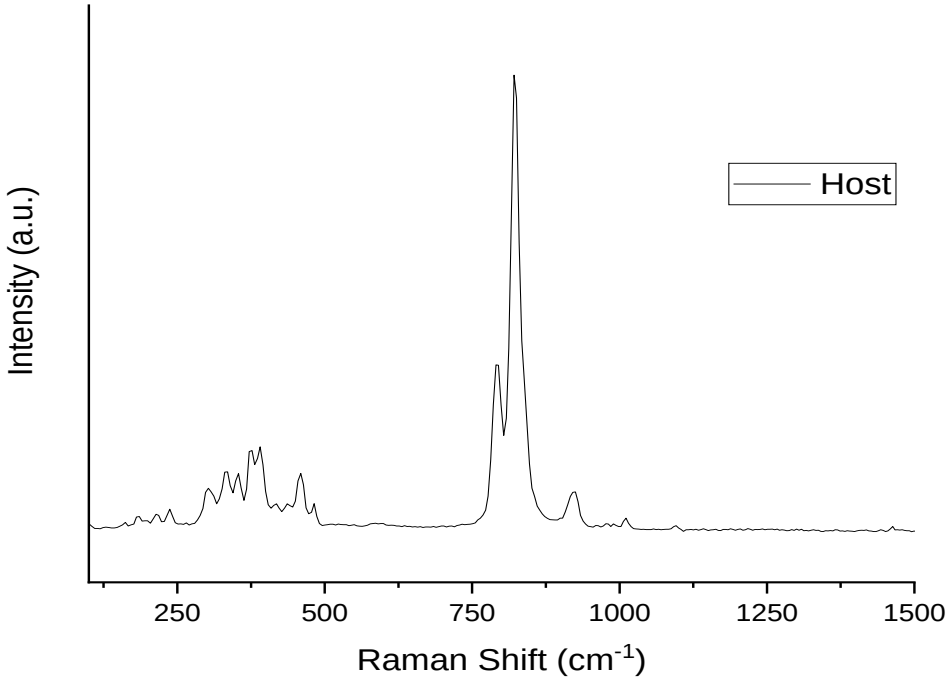

Figure 4.5: The Raman spectrum of Li_3VO_4 (host)

Figure 4.6a shows the Raman spectra of $Li_{3-x}Na_xVO_4$ ($0 \leq x \leq 0.1$) material synthesized by the citrate sol-gel method at 600 °C. It shows bands stretching and bending vibrations of V–O modes in VO_4 tetrahedra. The stretching and bending modes were, respectively, detected at 825 and 303 cm^{-1} for Li_3VO_4. The main Raman peaks appear at around 794 and 825 cm^{-1}, which are due to the VO_4 tetrahedra vibrations. Well-defined Raman modes are observed for undoped and sodium doped LVO in the lower energy part of the spectra, that is, around 250 – 500 cm^{-1}. In the 500 – 750 cm^{-1} region, there are no Raman structures that are present. From the Raman spectra, it can be seen that doping of LVO does not introduce new intense Raman modes, and thus no impurity phases can be detected.

© University of Venda

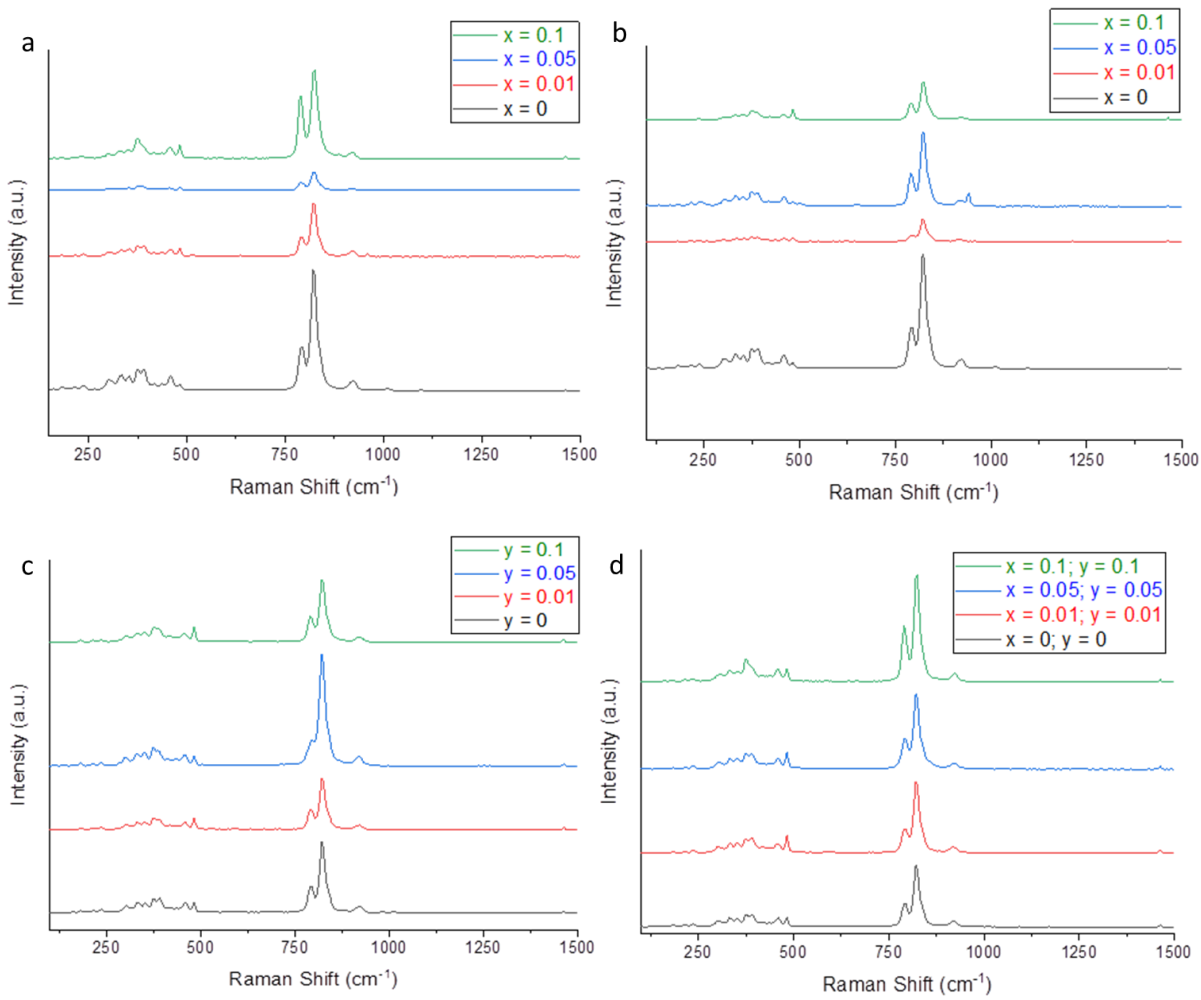

Figure 4.6: The Raman spectra of (a) $Li_{3-x}Na_xVO_4$ (b) $Li_{3-x}K_xVO_4$ (c) $Li_3V_{1-y}Cr_yO_4$ and (d) $Li_{3-x}K_xV_{1-y}Cr_yO_4$ doped at x = 0, 0.01, 0.05, 0.1 and y = 0, 0.01, 0.05, 0.1

In the potassium doped LVO Raman spectra (Figure 4.6b), there are no new peaks that can be observed concerning the host, that is, Li_3VO_4. Potassium doping does not influence the vibrations of vanadium tetrahedra. The spectra have also been collected from different points of the powder to test the sample homogeneity. No difference among spectra was detected during Raman mapping, indicating a high degree of homogeneity and the absence of impurity phases. Varying the potassium doping content (x) of LVO does not introduce any new peaks. Therefore, doping with potassium does not change the structure of the lithium vanadate.

The Raman spectra of the pure and Cr-doped Li_3VO_4 samples are reported in Figure 4.6c. Among the Raman peaks present in the spectra of pure and doped-LVO, two peaks at ~ 794 and ~ 825 cm^{-1} are much stronger and sharper than the others, corresponding to vibrations of

© University of Venda

V–O in VO_4 tetrahedra. The peak at 921 cm^{-1} is the smaller one and can be accounted for by the Raman shift peak having a relation to the asymmetry stretching vibrational mode of VO_4 tetrahedrons. In the lower energy of the spectra, well-defined Raman peaks can be observed for the pure and Cr-doped LVO at approximately 335, 358, 372, 386, and 459 cm^{-1}. In the region of 600 – 750 cm^{-1}, there are no Raman structures that are present. The doping of lithium vanadate with chromium does not introduce new intense Raman peaks, and also no impurities can be detected.

In Figure 4.6d, Raman spectra for the pure and co-doped lithium vanadate samples are reported in the energy region 100 – 1500 cm^{-1}. The main features are observable in two different vibrational energy ranges. In the high energy part of the spectra, the most intense Raman peaks are measured at approximately 794 and 825 cm^{-1}. An additional weaker Raman peak is observed at approximately 925 cm^{-1}. In the frequency region between 250 and 500 cm^{-1}, other significant Raman peaks are measured. To test the sample homogeneity, the spectra have been collected from different points of the powder. No difference among the spectra was detected during the Raman mapping and this indicated a high degree of homogeneity and absence of impurity phases. It can be said that co-doping lithium vanadate with potassium and chromium does not introduce new intense Raman modes. This means that co-doping lithium vanadate with K and Cr did not change the host structure.

© University of Venda

4.1.4 SEM-EDS

The EDS spectrum was taken to identify the chemical composition of Li_3VO_4 (LVO). Figure 4.7 below represents the EDS spectrum of LVO. As seen from the spectrum, the elemental presence of vanadium and oxygen were confirmed. A carbon peak is also present in the EDS spectrum since it was used as a conducting film during the analysis. No other peaks of impurities were detected suggesting that the prepared lithium vanadate material is impurity phase free.

EDS has limitation of detecting very light elements, especially those with atomic number lower than that of sodium. In this analysis, Lithium could not be detected because it is a very light element with atomic number 3 and the EDS instrument used can only detect elements from beryllium.

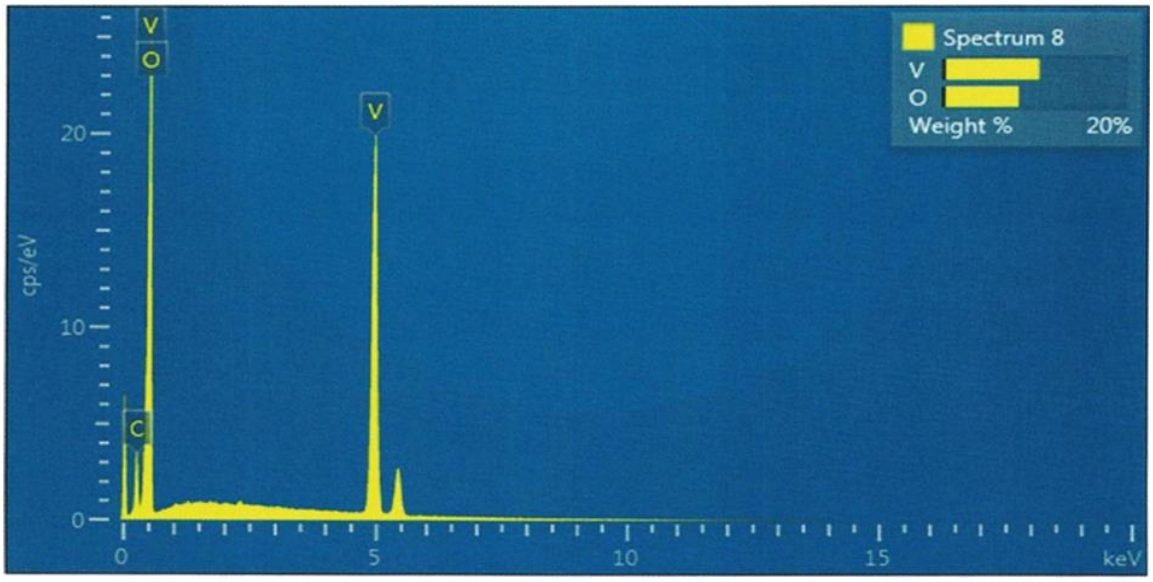

Figure 4.7: EDS spectrum of Li_3VO_4 (host) annealed at 600 ℃ for 3 hrs

To confirm the compositional distribution of the constituent elements of the powder samples, EDS mapping was used and their images are displayed in Figure 4.8. The EDS analysis of the Li_3VO_4 (host) is illustrated in Figure 4.7. Images of individual elements are displayed below the layered image, and they show that all elements are homogeneously distributed.

© University of Venda

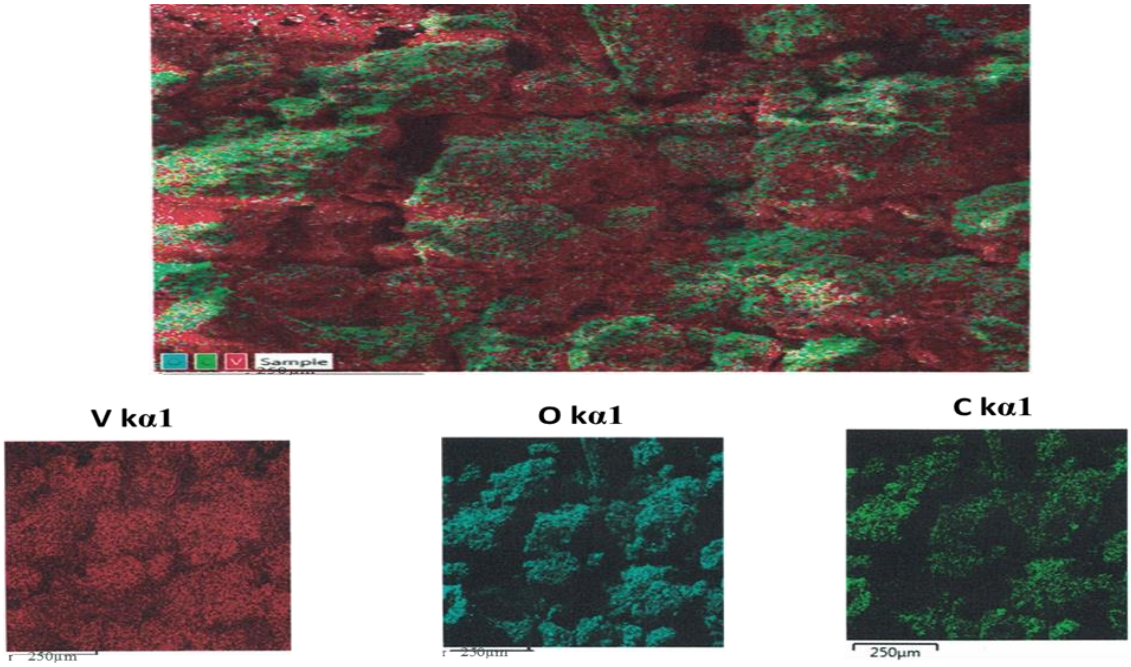

Figure 4.8: SEM image with corresponding EDS elemental mappings of LVO annealed at 600 ℃ for 3 hrs

Figure 4.9 shows the morphological aspect of the undoped Li_3VO_4 (host) which was examined using SEM. The SEM micrograph reveals that the morphology consists of a smooth surface with few irregular shapes. It can be observed that the particle size of the compound is not uniformly distributed in size and the particle size of the compound is approximately 2 µm. It can also be observed that agglomeration takes place among the particles.

© University of Venda

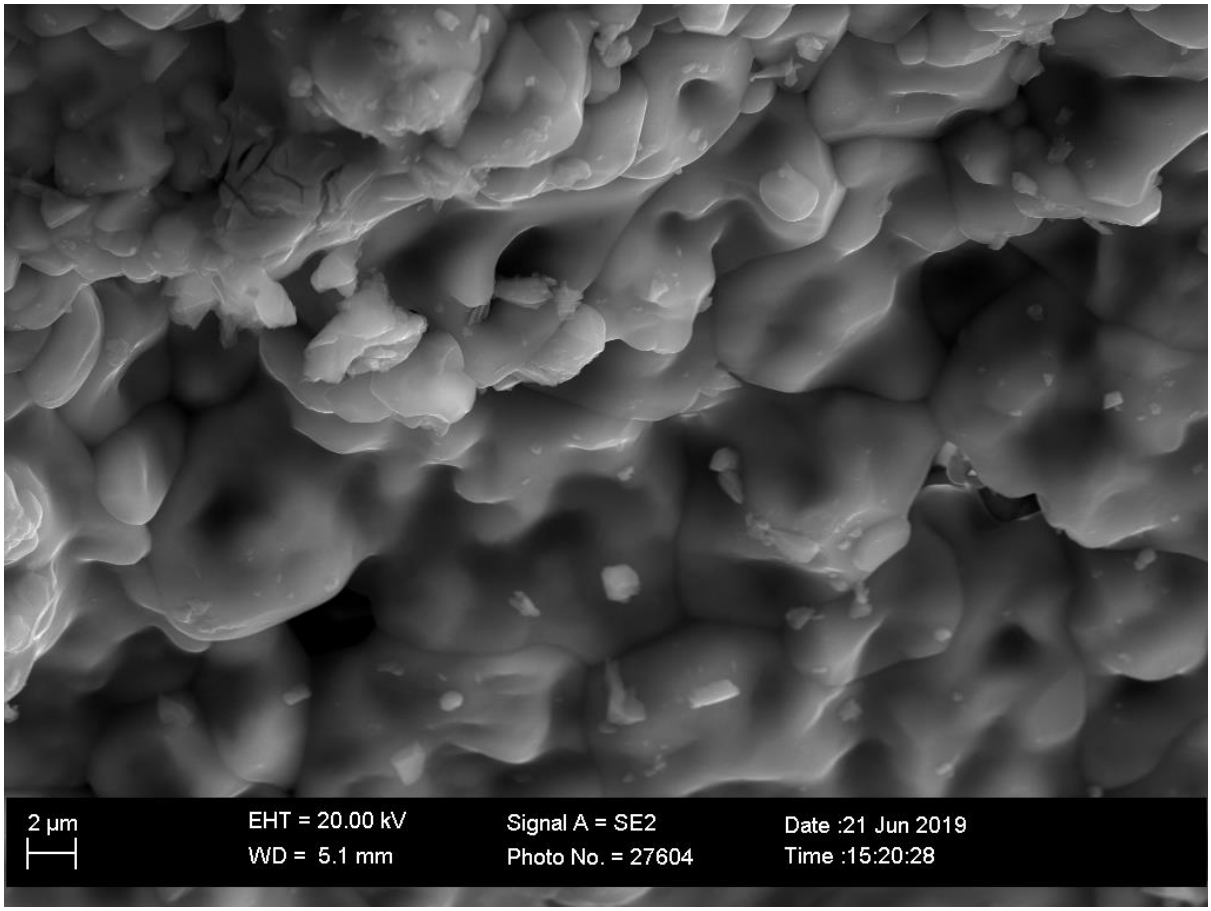

Figure 4.9: The SEM images of Li_3VO_4 (LVO) sample

Energy dispersive X-ray spectroscopy was used to identify the chemical composition of the samples. Figure 4.10 shows the EDS spectra of sodium doped lithium vanadate with sodium concentration varying from 0.01 to 0.1M. As seen from the Figure, the elemental presence of vanadium, oxygen, and sodium were confirmed. However, the presence of lithium could not be detected from the EDS analysis, this is because lithium is a light metal and produces low energy characteristic radiations. Hence, other techniques like Li NMR or XPS can be used to identify the presence of lithium, the presence of copper peaks in Figure 4.10c may suggest that $Li_{2.90}Na_{0.1}VO_4$ sample is not highly pure (Li *et al*, 2008). Alternatively, copper may have emanated from the starting material.

© University of Venda

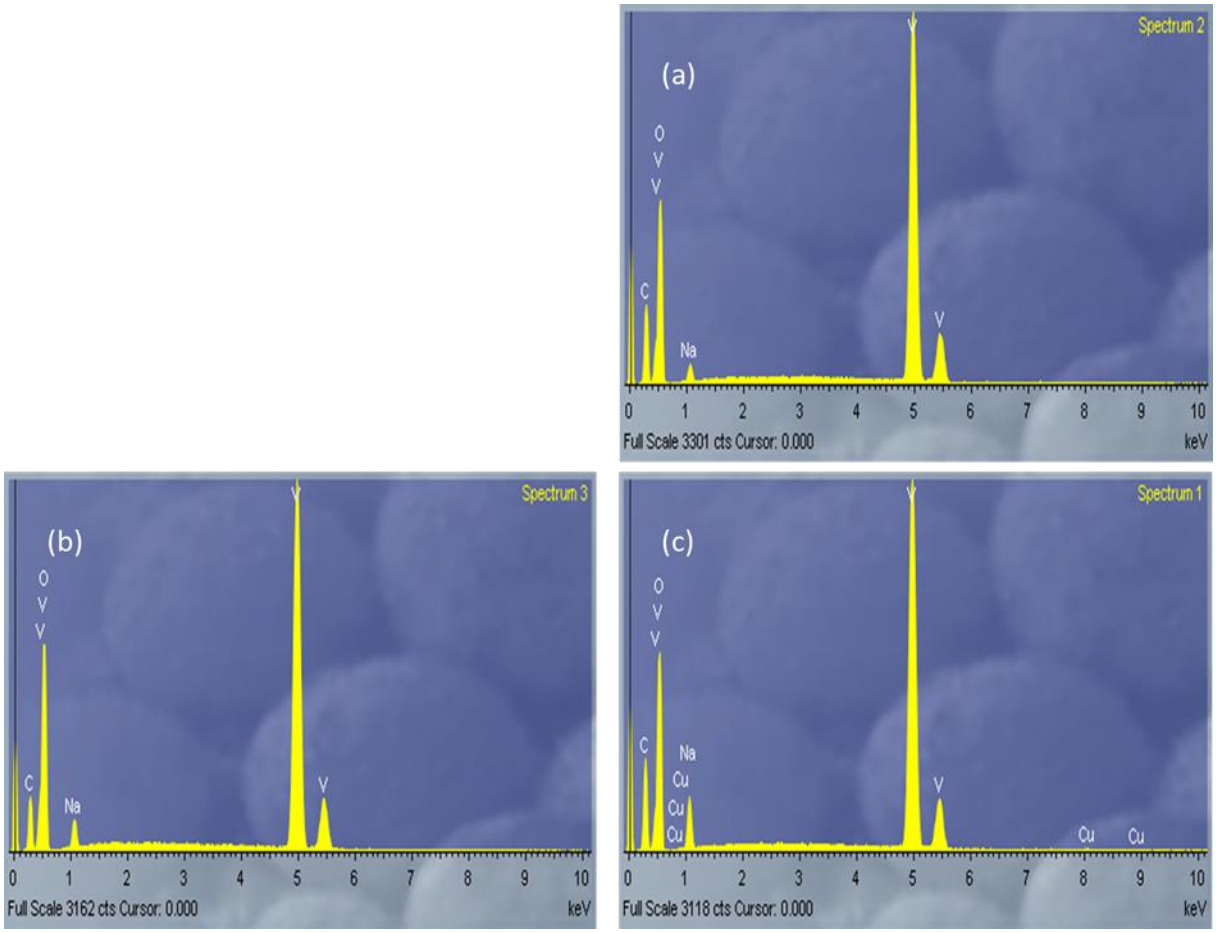

Figure 4.10: The EDS spectra of $Li_{3-x}Na_xVO_4$ doped at x = 0, 0.01, 0.05 and 0.1

Figure 4.11 shows the SEM images of undoped and sodium-doped lithium vanadate (LVO) powders prepared via the citrate sol-gel method. Figure 4.11a gives the SEM image of Li_3VO_4 (undoped). It can be observed that the particle size of the compound is not uniformly distributed in size. The particles have an average size of around 2 µm and agglomeration among the particles can be observed. For the Na-doped samples, Figure 4.11 (b-d), the particle size for all three samples is slightly smaller and a reduction in agglomeration can also be observed. As the sodium doping content increases, there is a decrease in particle size.

© University of Venda

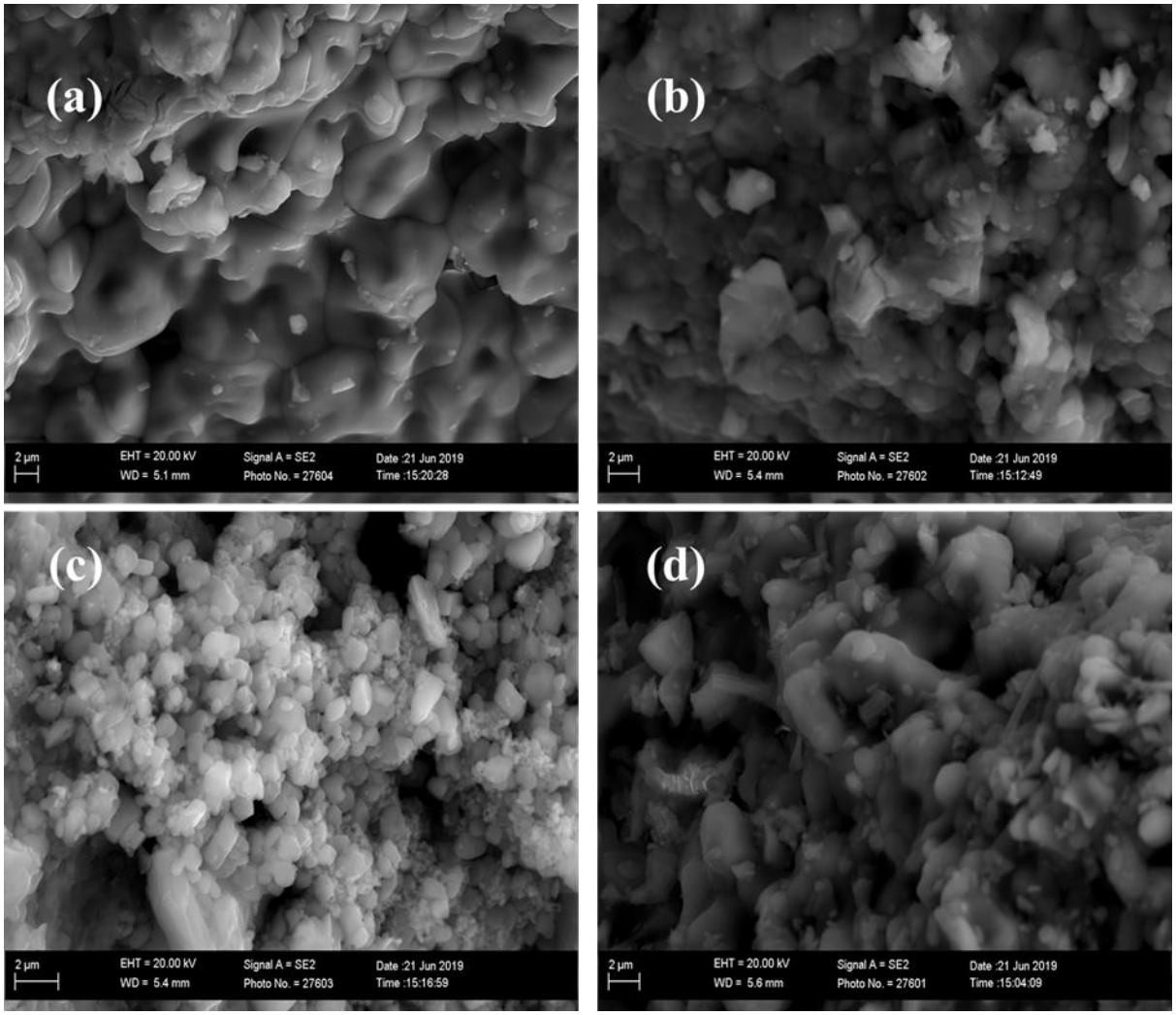

Figure 4.11: The SEM images of (a) LVO sample (b) $Li_{2.99}Na_{0.01}VO_4$ sample (c) $Li_{2.95}Na_{0.05}VO_4$ sample and (d) $Li_{2.90}Na_{0.1}VO_4$ sample

The EDS spectra were taken for all the synthesized undoped and doped LVO samples to identify the chemical composition. Figure 4.12 illustrates the EDS spectra for $Li_{3-x}K_xVO_4$ ($0 \leq x \leq 0.1$). As seen from Figure 4.12, the elemental presence of vanadium, oxygen, and substituted potassium were confirmed. However, the presence of lithium could not be detected from EDS analysis, this is because, lithium is a light metal and produces low energy characteristic radiations. Therefore, other techniques like XPS or Li NMR are required to identify the presence of lithium.

© University of Venda

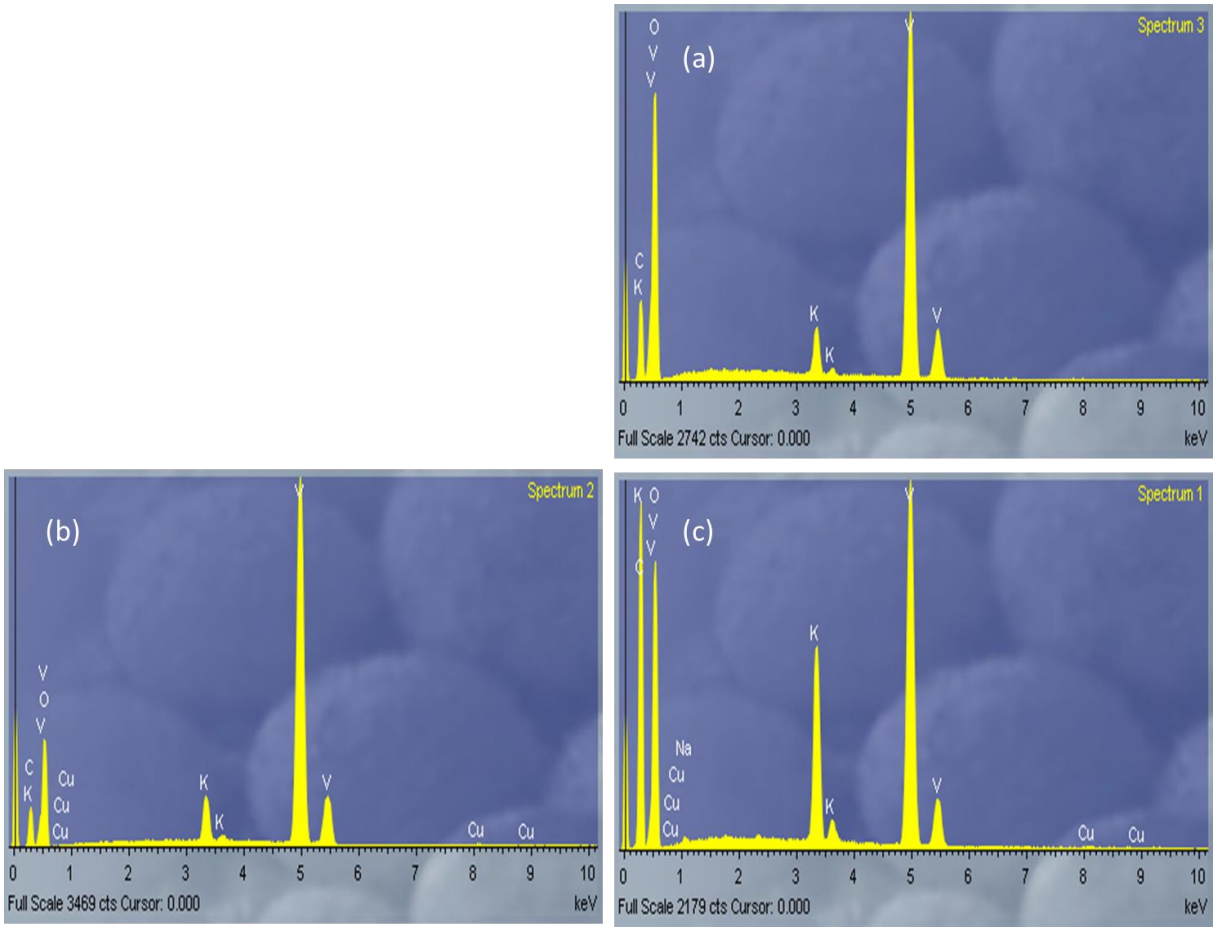

Figure 4.12: The EDS spectra of $Li_{3-x}K_xVO_4$ doped at x = 0.01, 0.05 and 0.1

To explain the structural aspects of undoped and potassium-doped lithium vanadate powders in detail, SEM images are exhibited in Figure 4.13. The SEM image shown in Figure 4.13a indicates that the potassium-free sample (Li_3VO_4) holds non-uniform particles with the particle size of approximately 2 µm, which is much larger than that of potassium-doped samples (Figure 4.13 b-d) of approximately 500 nm. It can be seen that the LVO sample consists of agglomerations of widely dispersed small particles. However, for the K-doped LVO, the samples have a decrease in agglomeration as a concentration of potassium dopant increases.

© University of Venda

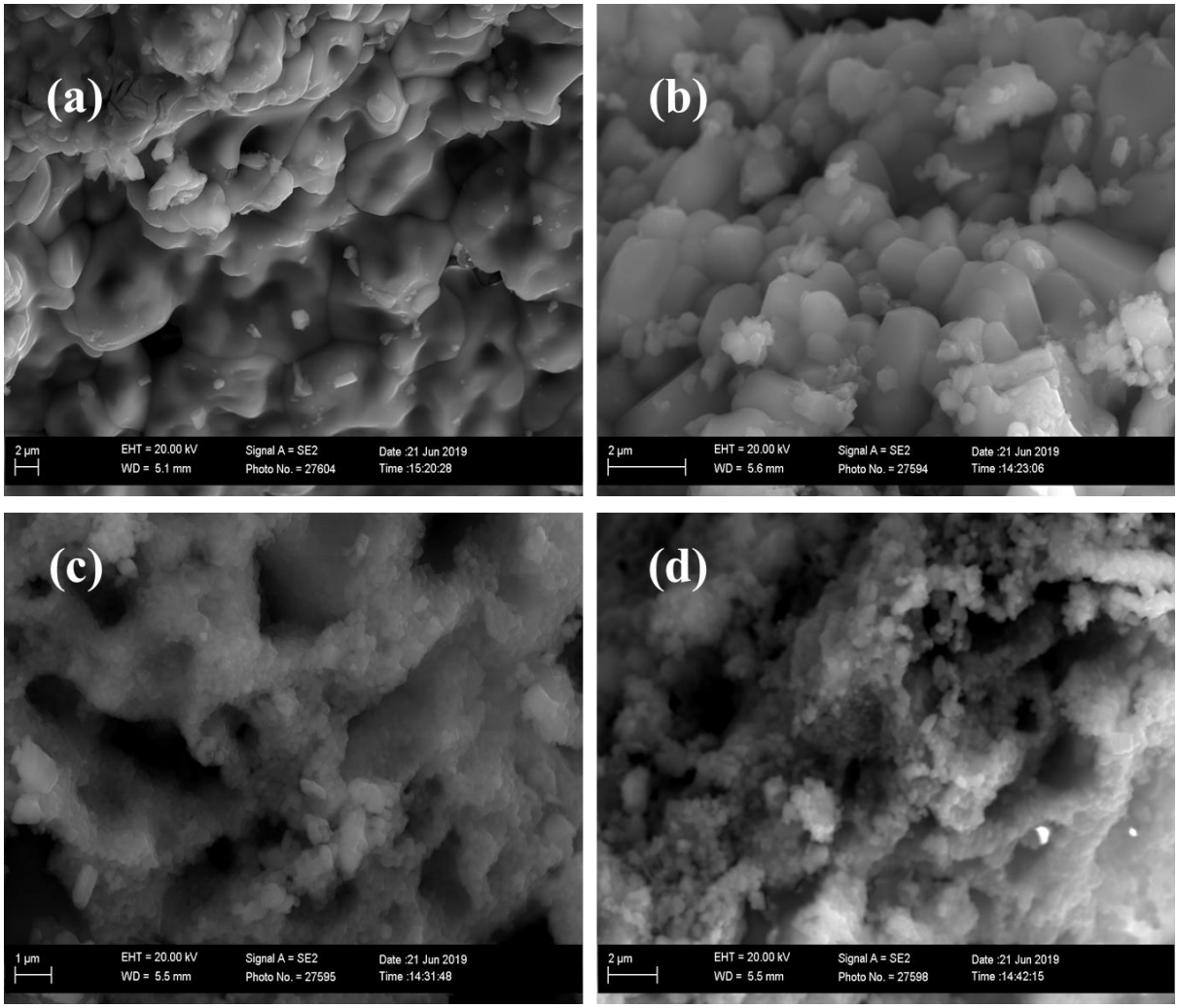

Figure 4.13: The SEM images of (a) LVO sample (b) $Li_{2.99}K_{0.01}VO_4$ sample (c) $Li_{2.95}K_{0.05}VO_4$ sample and (d) $Li_{2.90}K_{0.1}VO_4$ sample

The EDS spectra were taken to identify the chemical composition of chromium doped lithium vanadate ($Li_3V_{1-y}Cr_yO_4$). Figure 4.14 (a – c) shows the presence of chromium, vanadium, and oxygen. Lithium, however, could not be detected. This is because it is a light metal hence produces low energy characteristic radiations. The absence of the impurity peaks suggests that the sample obtained is highly pure.

© University of Venda

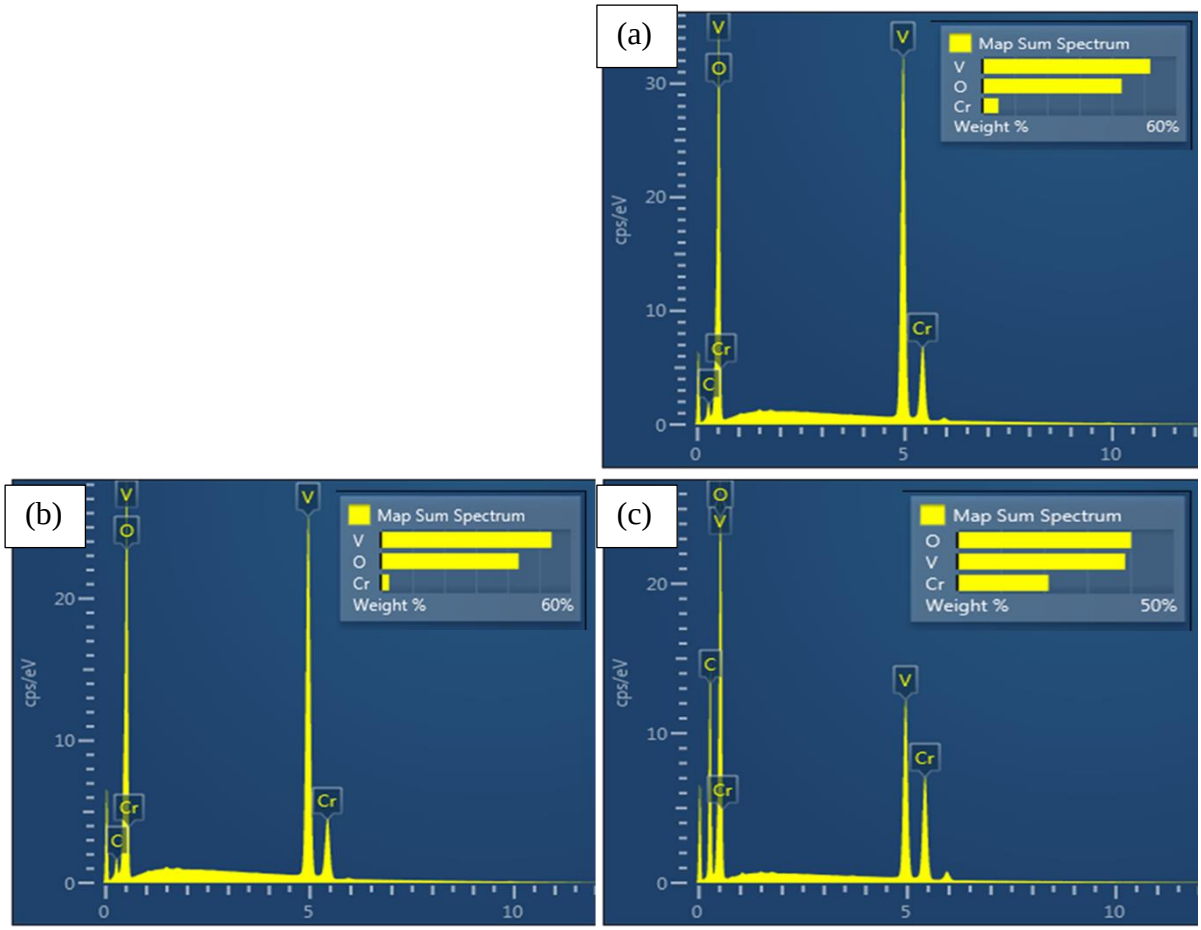

Figure 4.14: The EDS spectra of $Li_3V_{1-y}Cr_yO_4$ doped at (a) x = 0, (b) 0.01, (c) 0.05 and (d) 0.1

To confirm the compositional distribution of the constituent elements of the powder samples, EDS mapping was used and their images are displayed in Figure 4.15. The EDS analysis of the $Li_3V_{1-y}Cr_yO_4$ (where y = 0.01) is illustrated in Figure 4.15 (a). Images of individual elements are displayed along with the layered image, and they show that all elements are homogeneously distributed. Figure 4.15 (b) shows the EDS analysis of the $Li_3V_{1-y}Cr_yO_4$ (where y = 0.05), the layered image, and the images of individual elements also show that the constituent elements are homogeneously distributed. Figure 4.15 (c) shows the EDS analysis of the $Li_3V_{1-y}Cr_yO_4$ (where y = 0.1), the layered image, and the images of individual elements also show that the constituent elements are homogeneously distributed.

© University of Venda

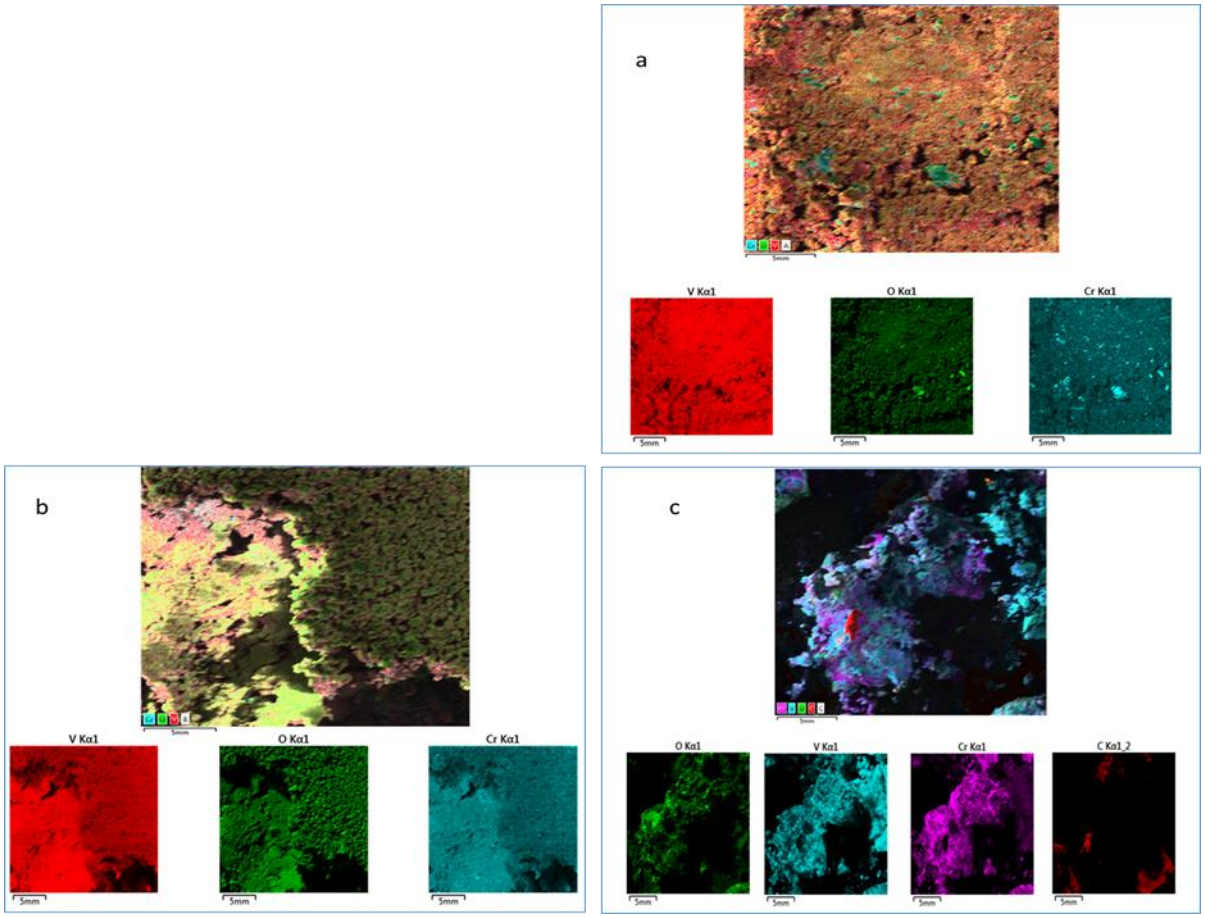

Figure 4.15: The EDS mapping images for (a) $Li_3V_{1-y}Cr_yO_4$ (where y = 0.01) (b) $Li_3V_{1-y}Cr_yO_4$ (where y = 0.05) and (c) $Li_3V_{1-y}Cr_yO_4$ (where y = 0.1)

Figure 4.16 shows SEM images of the $Li_3V_{1-y}Cr_yO_4$ (y = 0, 0.01, 0.05 and 0.1) powders. It can be seen that the particle size of the compound are not the same. The particle has an average size of around 5 µm. As the concentration of the dopant (Cr) increases, the clustering together of the particles decreases. From Figure 4.17a, the particle size is approximately 2 µm and for the chromium-doped LVO. Figure 4.16 (b – d), the particle size ranges from 0.5 – 1 µm.

© University of Venda

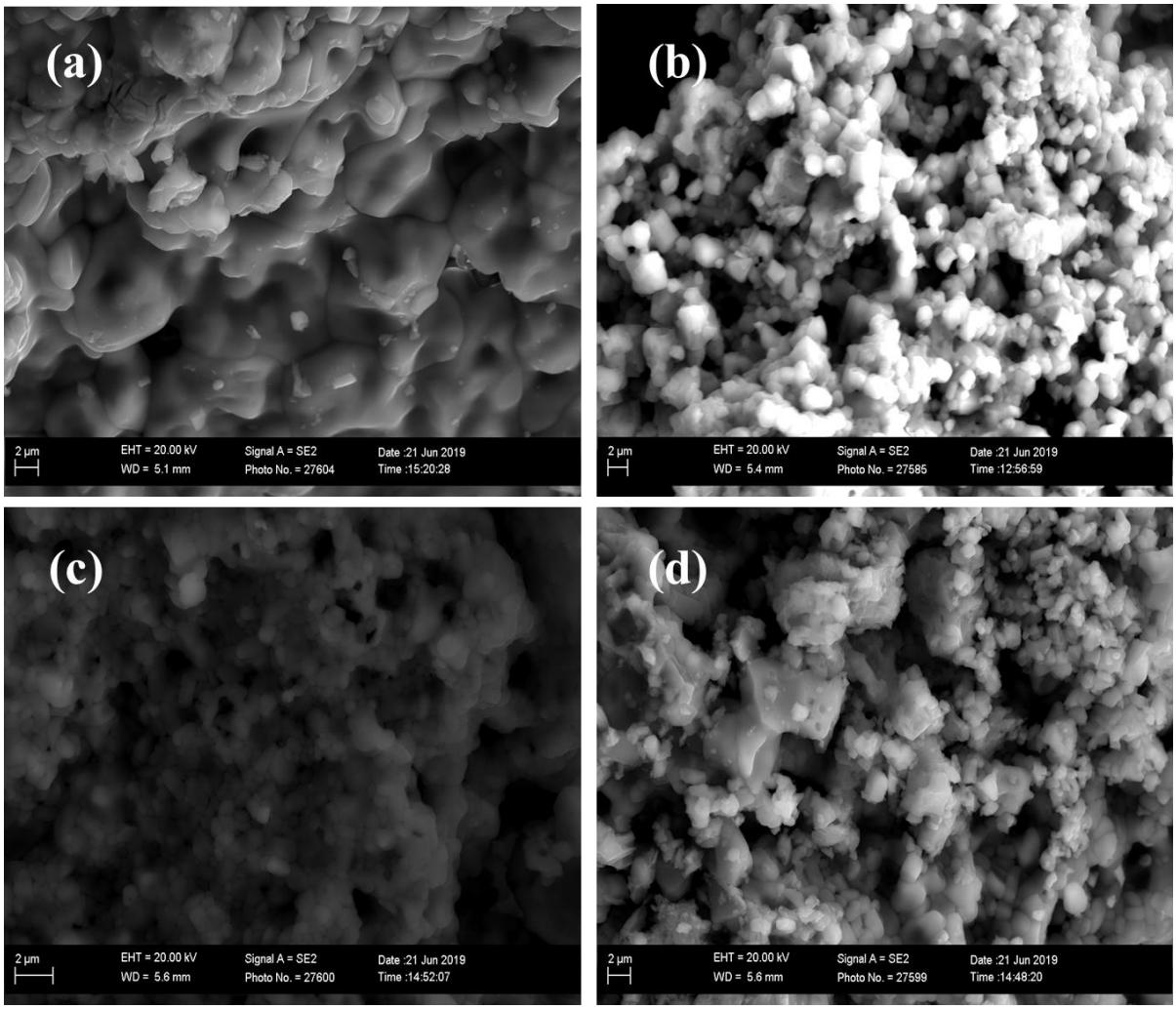

Figure 4.16: The SEM images of (a) LVO sample (b) $Li_3V_{0.99}Cr_{0.01}O_4$ sample (c) $Li_3V_{0.95}Cr_{0.05}O_4$ sample and (d) $Li_3V_{0.9}Cr_{0.1}O4$ sample

The EDS spectra are shown in Figure 4.17 (a) – (c). The EDS spectra show the presence of vanadium, oxygen, potassium, and chromium elements in the prepared samples. However, in Figure 4.17 (a), chromium is not present and this may be due to the low concentration (0.01M) of Cr used as compared to other samples.

© University of Venda

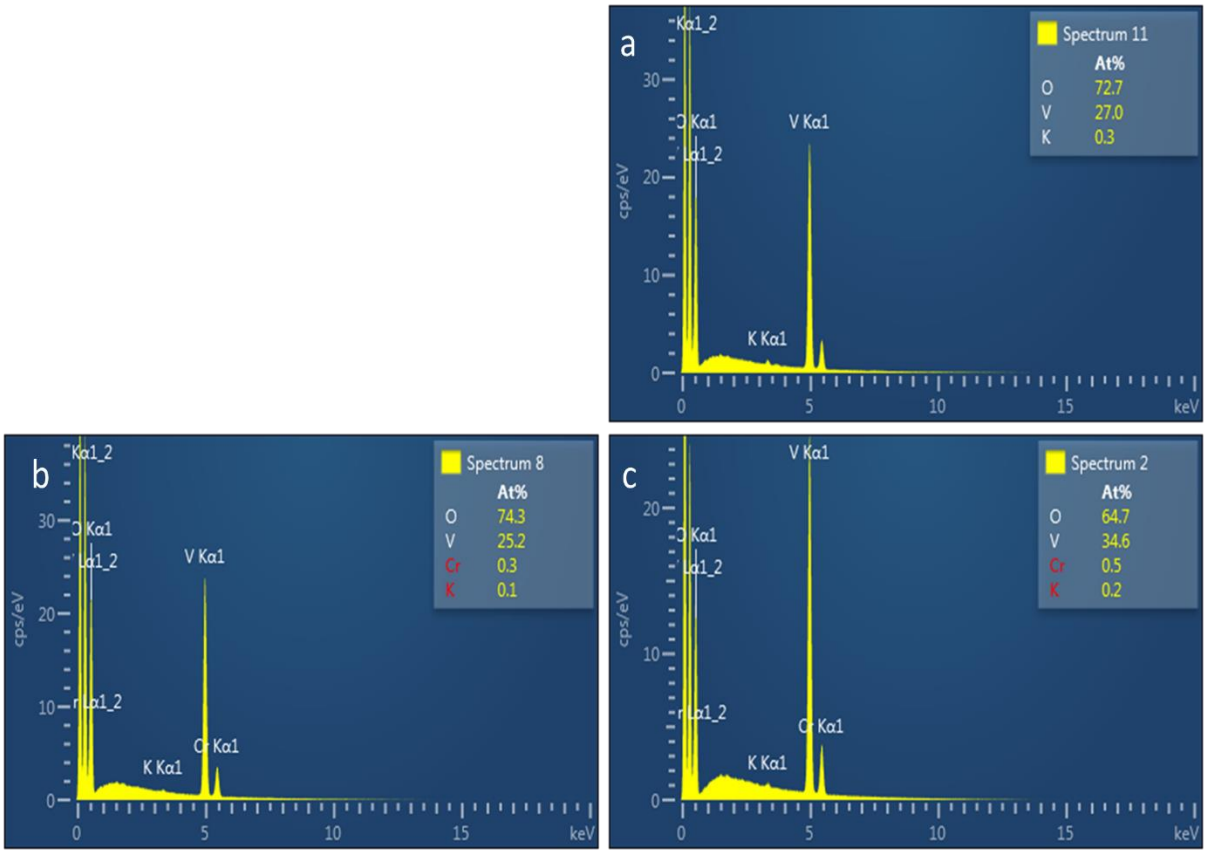

Figure 4.17: The EDS spectra of (a) $Li_{2.99}K_{0.01}V_{0.99}Cr_{0.01}O_4$ (b) $Li_{2.95}K_{0.05}V_{0.95}Cr_{0.05}O_4$ and (c) $Li_{2.90}K_{0.1}V_{0.9}Cr_{0.1}O4$ samples

Figure 4.18 shows the scanning electron microscopy images of doped and undoped Li_3VO_4 (LVO) powders. The studied samples show a variety of particle morphologies as displayed in the images. For LVO, a great deal of smaller particles were agglomerated to form a much larger particle and the size of the larger particle is about 1.5 µm, whereas the smaller particle has a particle size of 600 nm. However, such an agglomeration has decreased in the co-doped LVO samples. The K and Cr-doped LVO have a similar morphology but its size decreased considerably and the particle size is about 200 nm. Such a decrease in particle size in the KCr-doped $Li_{3-x}K_xV_{1-y}Cr_yO_4$ (x = 0.01, 0.05, 0.1 and y = 0.01, 0.05, 0.1) samples can lead to a sufficient contact between the electrolyte and the active materials in the battery. This may result in the favourable diffusion and transmission of the Li^+ in the electrode.

© University of Venda

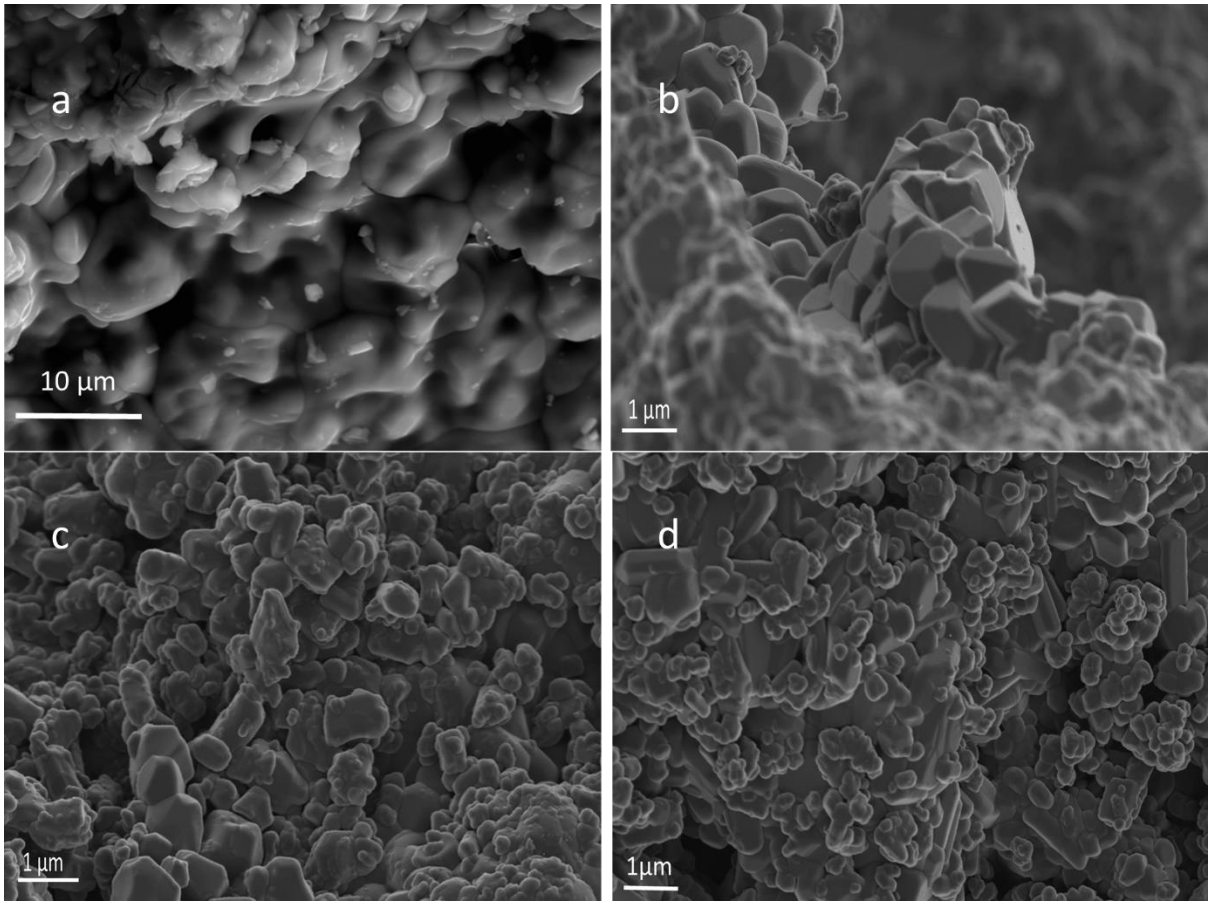

Figure 4.18: The SEM images of (a) LVO sample (b) $Li_{2.99}K_{0.01}V_{0.99}Cr_{0.01}O_4$ sample (c) $Li_{2.95}K_{0.05}V_{0.95}Cr_{0.05}O_4$ sample and (d) $Li_{2.90}K_{0.1}V_{0.9}Cr_{0.1}O4$ sample

© University of Venda

Chapter 5: Conclusion and Recommendations

5.1 Conclusion

Using oxides, carbonates and nitrates, the undoped Li_3VO_4, singly doped $Li_{3-x}Na_xVO_4$, $Li_{3-x}K_xVO_4$, $LiV_{1-y}Cr_yO_4$ and co-doped $Li_{3-x}K_xV_{1-y}Cr_yVO_4$ (where x = 0.01, 0.05 & 0.1; y = 0.01, 0.05 & 0.1) nanomaterials were successfully synthesized via citrate sol-gel method. The structure and morphology of samples are characterised by XRD, Raman, FTIR, and SEM. Few important observations of the research are concluded below:

XRD data revealed that all synthesized materials reported in this work crystallized as a single phase with an orthorhombic crystal structure of the Pmn21 space group. Sodium doping revealed that sodium ions entered into the lattice successfully and this resulted in an expanded lattice. Doping with alkali cations (Na^+ and K^+) showed a slight increase of lattice parameters a, b, and c as concentration of the dopant increases. The main reason why Na^+ and K^+ ions occupies the Li-site rather than the vanadium site is because of different ionic radius and ionic valence state. The ionic radius of Na^+, K^+ and Li^+ are 0.99 Å, 1.33 Å and 0.68 Å, respectively. There is significantly smaller difference between ionic radius of Na^+, K^+ and Li^+ ions. Additionally, the valence state between V^{5+}, K^+ and V^{5+}, Na^+ is significantly larger as compared to that of Li^+, K^+ and Li^+, Na^+. Therefore, K^+ and Na^+ occupied the lithium site more easily for the formation of single phase and stable LVO. Vanadium site was occupied by Cr^{3+} ion rather than lithium site because of different ionic radius and ionic valence state. Singly or co-doping of LVO with alkali metals (Na and K) and/or transition metal (Cr) does not introduce impurity phases on the XRD spectra.

From the FTIR analysis, one distinct strong absorption peak which is associated with the stretching mode of VO_4 is detected. Compared with the host (Li_3VO_4), the IR bands for the K-doped LVO samples are shifted slightly towards lower wavenumber.

In Raman analysis, two strongest Raman peaks associated with the stretching vibrations of VO_4 tetrahedra are observed for all synthesized powder materials. Doping does not introduce new intense Raman peaks.

© University of Venda

EDS study demonstrates that the element of V, O, and substituted Na, K, and/or Cr shows a very uniform distribution in $Li_3V_{1-y}Cr_yO_4$ (y = 0.01, 0.05, and 0.1). The influence of doping on the morphology of LVO powder samples was revealed by SEM. For pure LVO, the particles of the sample are agglomerated, having different sizes. However, for the Na-doped LVO, K-doped LVO, Cr-doped LVO, and KCr-doped LVO, the degree of agglomeration has decreased. It is a fact that uniformity and size of particle of the electrode materials often play an important role in improving the electrochemical properties. Therefore, better performance are predicted for in the doped LVO with small and uniform particle sizes.

5.2 Recommendations

As far as the current study is concerned, and for prospects, it is recommended that the following aspects are investigated:

- To study the effects of citric acid content in the undoped and doped lithium vanadates
- To study the effects of annealing temperatures in the undoped LVO, sodium doped LVO, potassium doped LVO chromium doped LVO, and co-doped LVO with potassium and chromium
- To study the effects of sodium and chromium concentrations in the co-doped lithium vanadates $Li_{3-x}Na_xV_{1-y}Cr_yVO_4$
- To perform electrochemical testing on the synthesized undoped, doped and co-doped lithium vanadate products
- Because lithium is a light metal and produces low energy characteristic radiations other techniques like Li NMR or XPS can be used to identify the presence of lithium

© University of Venda

References

Agrawal, K., Singh, G., Puri, D., and Prakash, S., (2016). Synthesis And Characterization Of Hydroxyapatite Powder By Sol-Gel Method For Biomedical Application. *Journal Of Minerals And Materials Characterization And Engineering*, 10, pp.727 – 734.

Akhtar, K., Khan, S.A., Khan, S.B., and Asiri, A.M., (2018). Scanning Electron Microscopy: Principle And Application In Nanomaterials. *In Handbook Of Materials Characterization*, pp. 113 – 145.

Armand, M., and Tarascon, J.M., (2008). Building Better Batteries. *Nature*, *451*, pp.652 – 657.

Atalla, R.H., Agarwal, U.P., and Bond, J.S., (2012). 4.6 Raman Spectroscopy. *Methods In Lignin Chemistry*, pp.162 – 176.

Bhatt, M. D., and Dwyer, C. O., (2015). Recent Progress In Theoretical And Computational Investigations Of Li-Ion Battery Materials And Electrolytes. *Physical Chemistry Chemical Physics*,*17*, pp.4799 – 4844.

Bellis M., (2012). How A Battery Works. About.Com Inventors. Web 19 October 2016. http://inventors.about.com/od/bstartinventions/ss/how-a-battery-works.htm#showall

Bensalah, N., and Dawood, H., (2016). Review On Synthesis, Characterization, And Electrochemical Properties Of Cathode Materials For Lithium Ion Batteries. *Journal Of Material Science & Engineering*, 5, pp.258 – 279.

Bhatt, M. D., and O'Dwyer, C., (2015). Recent Progress In Theoretical And Computational Investigations Of Li-Ion Battery Materials And Electrolytes. *Physical Chemistry Chemical Physics*, *17*, pp.4799 – 4844.

Bhuvaneswari, M.S., Selvasekarapandian, S., Kamishima, O., Kawamura, J., and Hattori, T., (2005). Vibrational Analysis Of Lithium Nickel Vanadate. *Journal Of Power Sources*, *139*, pp.279 – 283.

Bonheur K., (2016). Lithium Ion Battery: Advantages And Disadvantages. Version Daily. Web 17 September 2017. http://www.versiondaily.com/lithium-ion-battery-advantages-disadvantages/

© University of Venda

Bowley, H.J., Gerrard, D.L., Louden, J.D., and Turrell, G., (2012). *Practical Raman Spectroscopy*. Springer Science & Business Media.

Bumbrah, G.S., and Sharma, R.M., (2016). Raman Spectroscopy–Basic Principle, Instrumentation And Selected Applications For The Characterization Of Drugs Of Abuse. *Egyptian Journal Of Forensic Sciences, 6*, pp.209 – 215.

Bunaciu, A.A., Udriştioiu, E.G., and Aboul-Enein, H.Y., (2015). X-Ray Diffraction: Instrumentation And Applications. *Critical Reviews In Analytical Chemistry*, *45*, pp.289 – 299.

Cao, G., (2004). *Nanostructures And Nanomaterials: Synthesis, Properties And Applications*. World Scientific.

Chakrabarti, S., Thakur, A.K., and Biswas, K., (2013). DFT Analysis Of Lithium De-Intercalation In Li_2FeVO_4. *Ionics*, *19*, pp.1515 – 1526.

Chakrabarti, S., Thakur, A.K., and Biswas, K., (2017). Synthesis, Characterization, And Cell Performance Of $Li_{0.5}fev_{1.5}O_4$. *Ionics*, pp.1 – 9.

Davison J., and Boyce J., (2012). Low Cost, Novel Methods For Fabricating All-Solid-State Lithium Ion Batteries. Bachelor Of Science In Chemical Engineering. Worcester Polytechnic Institute.

Dickson, D. L., and Ely, R. L., (2013). Silica Sol-Gel Encapsulation Of Cyanobacteria: Lessons For Academic And Applied Research. *Applied Microbiology And Biotechnology*, 97, pp.1809 – 1819.

Downes, A., and Elfick, A., (2010). Raman Spectroscopy And Related Techniques In Biomedicine. *Sensors*, *10*, pp.1871 – 1889.

Emsley, J., (2011). *Nature's Building Blocks: An A – Z Guide To The Elements*, Oxford University Press, New York

Feng, Y., Li, Y., and Hou., F., (2009). Preparation And Electrochemical Properties Of Cr Doped Liv_3o_8 Cathode For Lithium Ion Batteries. *Materials Letters*, 63, pp.1338 – 1340.

Fergus, J.W., (2010). Recent Developments In Cathode Materials For Lithium Ion Batteries. *Journal Of Power Sources*, *195*, pp.939 – 954.

Fu, Q., Du, F., Bian, X., Wang, Y., Yan, X., Zhang, Y., Zhu, K., Chen, G., Wang, C., and Wei, Y., (2014). Electrochemical Performance And Thermal Stability Of $Li_{1.18}Co_{0.15}Ni_{0.15}Mn_{0.52}O_2$

© University of Venda

Surface Coated With The Conic Conductor Li_3VO_4. *Journal Of Materials Chemistry A*, *2*, pp.7555 – 7562.

Goldstein, J. I., Newbury, D. E., Lyman, C. E., and Joy, D. C., (2017). *Scanning Electron Microscopy And X-Ray Microanalysis*. Springer.

Goodenough, J.B., and Kim, Y., (2009). Challenges For Rechargeable Li Batteries. *Chemistry Of Materials*, *22*, pp.587 – 603.

Guozhong, C., (2004). *Nanostructures And Nanomaterials: Synthesis, Properties And Applications*. World Scientific.

Jaggi, N., and Vij, D.R., (2006). Fourier Transform Infrared Spectroscopy. *In Handbook Of Applied Solid State Spectroscopy*. Springer, Boston, MA

Jian, Z., Zheng, M., Liang, Y., Zhang, X., Gheytani, S., Lan, Y., Shi, Y., and Yao, Y., (2015). Li_3VO_4 Anchored Graphene Nanosheets For Long-Life And High-Rate Lithium-Ion Batteries. *Chemical Communications*, *51*, pp.229 – 231.

Jiang, J., Li, H., Huang, J., Li, K., Zeng, J., Yang, Y., Li, J., Wang, Y., Wang, J., and Zhao, J., (2017). Investigation Of The Reversible Intercalation/Deintercalation Of Al Into The Novel Li_3VO_4@ C Microsphere Composite Cathode Material For Aluminum-Ion Batteries. *ACS Applied Materials & Interfaces*, *9*, pp.28486 – 28494.

Kalluri, S., (2016). Nano-Engineering And Advanced Characterizations Of Layered-Structure Electrode Materials For Lithium-Ion And Sodium-Ion Batteries. Doctor Of Philosophy Thesis, School Of Mechanical, Materials And Mechatronics Engineering, University Of Wollongong.

Kim, W.T., Jeong, Y.U., Lee, Y.J., Kim, Y.J., and Song, J.H., (2013). Synthesis And Lithium Intercalation Properties Of Li_3VO_4 As A New Anode Material For Secondary Lithium Batteries. *Journal Of Power Sources*, *244*, pp.557 – 560.

Lai, Q.Y., Lu, J.Z., Liang, X.L., Yan, F.Y., and Ji, X.Y., (2001). Synthesis And Electrochemical Characteristics Of Li–Ni Vanadates As Positive Materials. *International Journal Of Inorganic Materials*, *3*, pp.381 – 385.

Li, H., and Zhou, H., (2012). Enhancing The Performances Of Li-Ion Batteries By Carbon-Coating: Present And Future. *Chemical Communications*, *48*, pp.1201 – 1217.

© University of Venda

Li, H., Liu, X., Zhai, T., Li, D., and Zhou, H., (2013). Li_3VO_4: A Promising Insertion Anode Material For Lithium-Ion Batteries. *Advanced Energy Materials*, *3*, pp.428 – 432.

Li, Q., Sheng, J., Wei, Q., An, Q., Wei, X., Zhang, P., and Mai, L., (2014). A Unique Hollow Li_3VO_4/Carbon Nanotube Composite Anode For High Rate Long-Life Lithium-Ion Batteries. *Nanoscale*, *6*, pp.11072 – 11077.

Liang, Z., Lin, Z., Zhao, Y., Dong, Y., Kuang, Q., Lin, X., Liu, X., and Yan, D., (2015). New Understanding Of Li_3VO_4/C As Potential Anode For Li-Ion Batteries: Preparation, Structure Characterization And Lithium Insertion Mechanism. *Journal Of Power Sources*, *274*, pp.345 – 354.

Liao, C., Zhang, Q., Zhai, T., Li, H. And Zhou, H., (2017). Development And Perspective Of The Insertion Anode Li_3VO_4 For Lithium-Ion Batteries. *Energy Storage Materials*, 7, pp.17 – 31.

Liivat, A., and Thomas, J.O., (2010). A DFT Study Of Polyanion Substitution Into The Li-Ion Battery Cathode Material Li_2FeSiO_4. *Computational Materials Science*, *50*, pp.191 – 197.

Liu, C., Masse, R., Nan, X., and Cao, G., (2016). A Promising Cathode For Li-Ion Batteries: $Li_3V_2(PO_4)_3$. *Energy Storage Materials*, *4*, pp.15 – 58.

Liu, H., Wu, Y.P., Rahm, E., Holze, R., and Wu, H.Q., (2004). Cathode Materials For Lithium Ion Batteries Prepared By Sol-Gel Methods. *Journal Of Solid State Electrochemistry*, *8*, pp.450 – 466.

Liu, W., Oh, P., Liu, X., Lee, M.J., Cho, W., Chae, S., Kim, Y., and Cho, J., (2015). Nickel-Rich Layered Lithium Transition-Metal Oxide For High-Energy Lithium-Ion Batteries. *Angewandte Chemie International Edition*, *54*, pp.4440 – 4457.

Liu, Y., Zhou, X., and Guo, Y., (2009). Effects Of Fluorine Doping On The Electrochemical Properties Of LiV_3O_8 Cathode Material. *Electrochimica Acta*, *54*, pp.3184 – 3190.

Luo, W., (2016) Advanced Materials For Rechargeable Lithium-Oxygen Batteries. Doctor Of Philosophy Thesis, AIIM; University Of Wollongong.

Maphiri, V.M., Dejene, F.B., and Motloung, S.V., (2017). Effects Of Mg^{2+} Concentration On The Structure And Optical Properties Of $Mg_xal_2o_{3+\ X}$: 0.88% Cd^{2+} ($0.25 \leq X \leq 4.5$) Nano-Powders Synthesized Via Citrate Sol-Gel. *Results In Physics*, *7*, pp.3510 – 3521.

© University of Venda

Massarotti, V., Capsoni, D., Bini, M., Mustarelli, P., Chiodelli, G., Azzoni, C.B., Galinetto, P., and Mozzati, M.C., (2005). Transport And Structural Properties Of Pure And Cr Doped Li_3VO_4. *The Journal Of Physical Chemistry B*, *109*, pp.14845 – 14851.

Mcdowall, J., (2008). Understanding Lithium-Ion Technology. *Proceedings Of Battcon*.

Mo, J., Zhang, X., Liu, J., Yu, J., Wang, Z., Liu, Z., Yuan, X., Zhou, C., Li, R., Wu, X., and Wu, Y., (2017). Progress On Li_3VO_4 As A Promising Anode Material For Li-Ion Batteries. *Chinese Journal Of Chemistry*, *35*, pp.1789 – 1796.

Morey, G.W., and Niggli, P., (1913). The Hydrothermal Formation Of Silicates, A Review. *Journal Of The American Chemical Society*. *35*, pp.1086 – 1130.

Moskalyk, R.R., and Alfantazi, A.M., (2003). Processing Of Vanadium: A Review. Minerals Engineering, 16, pp.793 – 805.

Mulaudzi, I., Zhang, Y., Ndlovu, G.F., Wu, Y., Legodi, M.A., van Ree, T., (2020). Copper Doped Li_3VO_4 as Anode Material for Lithium-ion Batteries. *Electroanalysis*, 32, pp.2635 – 2641.

Ni, S., Lv, X., Ma, J., Yang, X., and Zhang, L., (2014). Electrochemical Characteristic Of Lithium Vanadate, Li_3VO_4 As A New Sort Of Anode Material For Li-Ion Batteries. *Journal Of Power Sources*, *248*, pp.122 – 129.

Ni, S., Lv, X., Ma, J., Yang, X., and Zhang, L., (2014). The Fabrication Of Li_3VO_4/Ni Composite Material And Its Electrochemical Performance As Anode For Li-Ion Battery. *Electrochimica Acta*, *130*, pp.800 – 804.

Ni, S., Zhang, J., Ma, J., Yang, X., and Zhang, L., (2015). Li_3VO_4/N-Doped Graphene With High Capacity And Excellent Cycle Stability As Anode For Lithium Ion Batteries. *Journal Of Power Sources*, *296*, pp.377 – 382.

Noerochim, L., Wang, J.Z., Wexler, D., Chao, Z., and Liu, H.K., (2013). Rapid Synthesis Of Free-Standing Moo_3/Graphene Films By The Microwave Hydrothermal Method As Cathode For Bendable Lithium Batteries. *Journal Of Power Sources*, *228*, pp.198 – 205.

Peterson, A.A., Vogel, F., Lachance, R.P., Fröling, M., Antal Jr, M.J., and Tester, J.W., (2008). Thermochemical Biofuel Production In Hydrothermal Media: A Review Of Sub-And Supercritical Water Technologies. *Energy & Environmental Science*, *1*, pp.32 – 65.

© University of Venda

Prabaharan, S.R.S., Yong, T.T., Fauzi, A., and Michael, M.S., (2001). Soft-Combustion Synthesis Of A New Cathode-Active Material, $Livwo_6$, For Lithium-Ion Batteries. *Journal Of Power Sources*, *97*, pp.535 – 540.

Prabakar, S.J., Hwang, Y.H., Bae, E.G., Shim, S., Kim, D., Lah, M.S., Sohn, K.S., and Pyo, M., (2013). Sno_2/Graphene Composites With Self-Assembled Alternating Oxide And Amine Layers For High Li-Storage And Excellent Stability. *Advanced Materials*, *25*, pp.3307 – 3312.

Qin, R., Shao, G., Hou, J., Zheng, Z., Zhai, T., and Li, H., (2017). One-Pot Synthesis Of Li_3VO_4@ C Nanofibers By Electrospinning With Enhanced Electrochemical Performance For Lithium-Ion Batteries. *Science Bulletin*, *62*, pp.1081 – 1088.

Rao, B.G., Mukherjee, D., and Reddy, B.M., (2017). Novel Approaches For Preparation Of Nanoparticles. In *Nanostructures For Novel Therapy*, pp. 1 – 36.

Ren, W., Yao, X., Niu, C., Zheng, Z., Zhao, K., An, Q., Wei, Q., Yan, M., Zhang, L., and Mai, L., (2016). Cathodic Polarization Suppressed Sodium-Ion Full Cell With A 3.3V High-Voltage. *Nano Energy*, *28*, pp.216 – 223.

Ren, W., Zheng, Z., Xu, C., Niu, C., Wei, Q., An, Q., Zhao, K., Yan, M., Qin, M., and Mai, L., (2016). Self-Sacrificed Synthesis Of Three-Dimensional $Na_3V_2(PO_4)_3$ Nanofiber Network For High-Rate Sodium–Ion Full Batteries. *Nano Energy*, *25*, pp.145 – 153.

Rui, X., Lu, Z., Yin, Z., Sim, D.H., Xiao, N., Lim, T.M., Hng, H.H., Zhang, H., and Yan, Q., (2013). Oriented Molecular Attachments Through Sol–Gel Chemistry For Synthesis Of Ultrathin Hydrated Vanadium Pentoxide Nanosheets And Their Applications. *Small*, pp.716 – 721.

Schroder, D.K., (2006). Semiconductor Material And Device Characterization. John Wiley & Sons.

Schutts S.M., and Kinney R.J. (2000). Methods For Making Lithium Vanadium Oxide Electrode Materials. US6136476.

Shi, Y., Wang, J., Chou, S., Wexler, D., Li, H., Ozawa, K., Liu, H., and Wu, Y. (2013). Hollow Structured Li_3VO_4 Wrapped With Graphene Nanosheets In Situ Prepared By One-Pot Template-Free Method As An Anode For Lithium-Ion Batteries. *Nano Letters: A Journal Dedicated To Nanoscience And Nanotechnology*, 13, pp.4715 – 4720.

© University of Venda

Skoog, D.A., Holler, F.J., and Crouch, S.R., 2017. *Principles Of Instrumental Analysis*. Cengage Learning.

Song, X., Jia, M., and Chen, R., (2002). Synthesis Of Li_3VO_4 By The Citrate Sol–Gel Method And Its Ionic Conductivity. *Journal Of Materials Processing Technology*, *120*, pp.21 – 25.

Thomas Jefferson Natural Accelerator Facility – Office Of Science Education, Its Elemental – The Periodic Table Of Elements. [Online]. Available From http://education.jlab.org/itselemental/ [Accessed 26 April 2021].

Ukessays. November 2018. Overview Of Infrared Spectroscopy. [Online]. Available From https://ukessays.com/essays/biology/an-overview-of-infrared-spectroscopy-biology-essay.php?vref=1 [Accessed 30 January 219].

Whittingham, M.S., (2004). Lithium Batteries And Cathode Materials. *Chemical Reviews*, *104*, pp.4271- 4302.

Wu, Y., (2015). *Lithium-Ion Batteries: Fundamentals And Applications.* British: CRC Press.

Yan, Z., Sun, Z., Xia, A., Yin, R., Huang, X., Yue, K., Xu, H., Zhao, G., and Qian, L., (2020). Li_3VO_4/Carbon Sheets Composites From Cellulose As An Anode Material For High Performance Lithium-Ion Batteries. *Ceramics International*, *46*, pp.2247 – 2254.

Yang, G., and Park, S.J., (2019). Conventional And Microwave Hydrothermal Synthesis And Application Of Functional Materials: A Review. *Materials*, *12*, pp.1177.

Yang, G., Zhang, B., Feng, J., Lu, Y., Wang, Z., Aravindan, V., Aravind, M., Liu, J., Srinivasan, M., Shen, Z., and Huang, Y., (2018). Morphology Controlled Lithium Storage In Li_3VO_4 Anodes. *Journal Of Materials Chemistry A*, *6*, pp.456 - 463.

Yoshimura, M., and Suda, H., (1994). Hydrothermal Processing Of Hydroxyapatite: Past, Present,, and Future. *Hydroxyapatite And Related Compounds*. Boca Raton (EE.UU): CRC Press Inc, pp.45 – 72.

Yoshino, A., (2012). The Birth Of The Lithium-Ion Battery. *Angewandte Chemie International Edition*, *51*, pp.5798 – 5800.

Zhang, C., Song, H., Liu, C., Liu, Y., Zhang, C., Nan, X., and Cao, G., (2015). Fast And Reversible Li Ion Insertion In Carbon-Encapsulated Li_3VO_4 As Anode For Lithium-Ion Battery. *Advanced Functional Materials*, *25*, pp.3497 – 3504.

© University of Venda

Zhang, C., Wang, K., Liu, C., Nan, X., Fu, H., Ma, W., Li, Z., and Cao, G., (2016). Effects Of High Surface Energy On Lithium-Ion Intercalation Properties Of Ni-Doped Li_3VO_4. *NPG Asia Materials*, *8*, P.E287.

Zhang, Z., (2015). Development Of Advanced Materials For Rechargeable Lithium-Ion Batteries, Doctor Of Philosophy Thesis, Institute For Superconducting & Electronic Materials, University Of Wollongong.

Zhen, M., Su, L., Yuan, Z., Liu, L., and Zhou, Z., (2013). Well-Distributed Tio_2 Nanocrystals On Reduced Graphene Oxides As High-Performance Anode Materials For Lithium Ion Batteries. *Rsc Advances*, *3*, pp.13696 – 13701.

Zhou, J., Zhao, B., Song, J., Chen, B., Ma, X., Dai, J., Zhu, X., and Sun, Y., (2018). The Enhanced Cycling Stability And Rate Capability Of Sodium-Modified Li_3VO_4 Anode Material For Lithium-Ion Batteries. *Solid State Ionics*, *322*, pp.30 – 38.

Zhu, Y., Wang, F., Liu, L., Xiao, S., Chang, Z., and Wu, Y., (2013). Composite Of A Nonwoven Fabric With Poly (Vinylidene Fluoride) As A Gel Membrane Of High Safety For Lithium Ion Battery. *Energy & Environmental Science*, *6*, pp.618 – 624.

Zou, Z., Liu, C., Jiang, X., Luo, J., Wang, X., and Feng, J., (2016). Hydrothermal Synthesis And Performance Of Co Doped Lithiated Vanadium Oxides As Cathode Material For Lithium Ion Batteries. In 2015 4th International Conference On Sensors. Measurement And Intelligent Materials. Atlantis Press.

© University of Venda